Received: 3 July 2020 | Revised: 20 October 2020 | Accepted: 22 October 2020

DOI: 10.1111/bre.12524

ORIGINAL ARTICLE

Basin Research | IAS EAGE | WILEY

Interplay of tectonics and magmatism during post-rift inversion on the central West Iberian Margin (Estremadura Spur)

Ricardo Pereira[1,2] | **Filipe Rosas**[2] | **João Mata**[2] | **Patrícia Represas**[3] | **Cláudia Escada**[4] | **Beatriz Silva**[5]

[1]Partex Oil and Gas, Lisbon, Portugal

[2]Instituto Dom Luiz (IDL), Faculdade de Ciências da Universidade de Lisboa, Lisbon, Portugal

[3]Laboratório Nacional de Energia e Geologia (LNEG), Amadora, Portugal

[4]Departamento de Engenharia Geográfica, Geofísica e Energia, Faculdade de Ciências, Universidade de Lisboa, Lisbon, Portugal

[5]Departamento de Geologia, Universidade de Lisboa, Lisbon, Portugal

Correspondence
Ricardo Pereira, Partex Oil and Gas, Rua Ivone Silva, 6, 1st floor, 1050-124 Lisbon, Portugal.
Email: ricardo.pereira@partex-oilgas.com

Abstract

The combined effects of post-rift magma emplacement and tectonic inversion on the hyper-extended West Iberian Margin are unravelled in detail using multichannel 2D/3D seismic data. The Estremadura Spur, acting as an uplifted crustal block bounded by two first-order transfer zones, shows evidence of four post-rift tectonic events each with a distinctive seismic-stratigraphic response that can be used to demonstrate the tectono-magmatic interplay, namely: (a) the Campanian onset of magmatism (including the Fontanelas Volcano, the widespread evidence of multiple sill complexes and the detailed description of a >20 km long laccolith, the Estremadura Spur Intrusion; (b) the Campanian-Maastrichtian NE-SW event pervasively affecting the area, resulting in regional uplift, reverse faulting and folding; (c) the Paleocene-mid Eocene inversion that resulted in widespread erosion and; (d) the Oligocene-mid Miocene evidence of rejuvenated NW-SE inversion marked by crestal faulting and forced-fault folding establishing the final geometry of the area. The distinct deformation styles within each tectonic phase document a case of decoupled deformation between Late Cretaceous and Tertiary units, in response to the predominant stress field evolution, revealing that the magnitude of Late Cretaceous inversion is far more significant than the one affecting the latter units. A detailed analysis of the laccolith and its overburden demonstrate the distinct deformation patterns associated both with magma ascent (including extensional faulting, forced-folding and concentric reverse faulting) and its interference as a rigid intrusive body during subsequent transpressive inversion. This reinforces the role that the combined tectono-magmatic events played on the margin. Also analysed is the wider impact of post-rift magmatism and the associate emplacement of sub-lithospheric magma on the rheology of a thinned continental crust. This takes into account the simultaneous tectonic inversion of the margin, the implied alternative views on characteristic heat flow, and on how these can be incorporated in source rock organic maturity modelling.

1 | INTRODUCTION

The West Iberian Margin (WIM; Figure 1), is a typical example of a magma-poor hyper-extended margin (e.g. Manatschal & Bernoulli, 1999; Tucholke et al., 2007). Despite the long-term focus on the significance of its evolving crustal architecture and related depositional successions during rifting, either at proximal and distal domains (Franke, 2013; Manatschal & Bernoulli, 1999; Péron-Pinvidic et al., 2013; Ravnås & Steel, 1998; Sutra et al., 2013; Whitmarsh et al., 2001; Wilson et al., 2001), multiple questions remain unclear. These include for example, the role of salt tectonics in controlling the overall evolution of the margin, how post-rift inversion affected dissimilarly its specific segments or on how Late Cretaceous magmatism on the decoupled crustal domain may have affected its thermal state and rheology. Nonetheless, recent research on the WIM brought forward new topics, such as the role of transcurrent zones in accommodating deformation resulting from the alternance of crustal plate polarity shifting from upper to lower plate setting (Pereira et al., 2017), or the deformable plate reconstruction of North Atlantic conjugate margins (e.g. Peace et al., 2019), have allowed a better constrain the controls of crustal inheritance in rift to post-rift evolution on passive margins.

Magmatic activity on passive margins is typically recorded at magma-rich domains, contrasting with neighbouring segments where the evidence of magma is scarce both in time and space, that is, magma-poor margins (Franke, 2013; Geoffroy, 2005). However, the magma-poor WIM is in some respects unique, as three magmatic cycles are described associated with different stages of its evolution and depicting distinct geochemical affinities and tectonic settings (see Mata et al., 2015 for a review). The first two are associated with rifting extension (Martins et al., 2008; Mata et al., 2015), whereas the latter, corresponds to a post-rift and syn-tectonic event dissimilarly affecting the continental and oceanic domains of the margin (Grange et al., 2010; Merle et al., 2009; Miranda et al., 2009). Geophysical models have been recently applied for the first time on the proximal margin to help characterising in detail some of the outcropping alkaline massifs (Neres et al., 2014; Ribeiro et al., 2013; Terrinha et al., 2017; Figure 1b), and to carry out gravimetry-magnetic modelling of conspicuous subsurface features off SW Iberia (Neres et al., 2018).

When compared with other known provinces where post-rift magmatic events occur, such as in Australia, the Atlantic North Sea or the South China Sea (Magee et al., 2013, 2017; Planke et al., 2017; Walker et al., 2020; Zhao et al., 2016), similar structural-magmatic manifestations are predominantly associated with the necking domain of magma-rich hyper-extended margins and are quasi coeval with lithospheric breakup (< 10 Ma after breakup). Contrastingly, on the proximal WIM the third magmatic cycle, with a unique sub-lithospheric alkaline signature (Grange et al., 2010; Miranda et al., 2009), occurred not only on a relatively thick continental crust segment of the stretched domain, but also post-dates lithosphere breakup in excess of 20 Ma.

Analysis of the offshore segments of the WIM, and specifically of the Estremadura Spur (ES; Figure 1), revealed that in this region the magmatism associated with the third cycle is abundant, comprising numerous sills, buried volcanic edifices and several voluminous plutonic intrusions (Escada et al., 2019; Miranda et al., 2010; Neres et al., 2014; Pereira et al., 2017; Pereira & Barreto, 2018; Simões et al., 2020). Nevertheless, all these features are still poorly investigated, requiring both new data and subsequent integrated analysis in order to gain a new overall insight on their tectono-magmatic evolution and possible geodynamic causes.

In this study, high-resolution seismic data (Figure 1), is used to unravel the characteristics of magmatic manifestations, devoting specific attention to the evidence of a laccolith (in excess of 20 km long) intruding the decoupled domain of the margin and to characterise in detail the distinct styles of deformation affecting the post-rift depositional sequences, not only during magma ascension, but also at a later time during the tectonic inversion of the margin. The present study also provides new insights regarding other key questions for the evolution of the WIM, namely: (a) What are the new age constraints for the magmatic occurrences on the submerged continental margin? (b) Are there any preferential pathways controlling the ascent of magma during the Late Cretaceous cycle? and, (c) What are the implications of this tectono-magmatic inheritance for the subsequent tectonic inversion of the margin? Finally, an overall discussion on the causes for the predominance of magmatic manifestations at specific segments of

Highlights

- West Iberian Margin shows combined effects of post-rift inversion and magmatism
- A laccolith intrusion is described using high-resolution seismic data
- The main tectono-magmatic event is shown to be of Late Cretaceous age
- Deformation between Late Cretaceous and the Tertiary is decoupled
- The interplay of tectonics and magmatism can be used as kinematic indicator

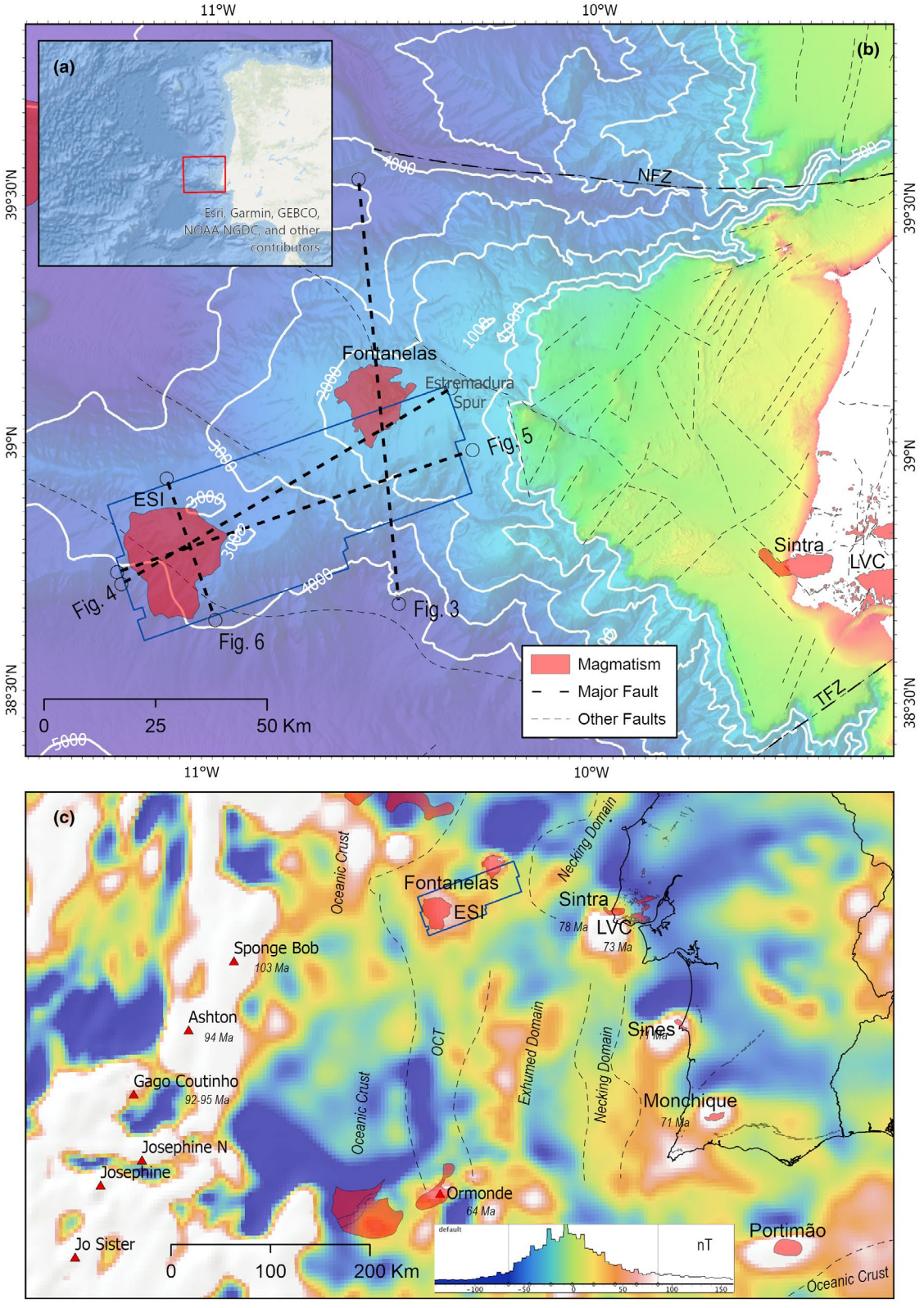

FIGURE 1 Location of the study area and the Estremadura Spur on the West Iberian Margin. (a) Atlantic location; (b) Location of seismic surveys and magmatic features on the Estremadura Spur. Faults based on Geological Map 1:1.000.000 (LNEG-LGM, 2010); ESI – Estremadura Spur Intrusion, NFZ – Nazaré Fault Zone, TFZ – Tagus Fault Zone; (c) Earth magnetic anomaly grid of South Iberia and the Atlantic (modified from GeoMappApp 3.3.0, EMAG2 2 min grid) and major evidence of Late Cretaceous magmatism (red triangles) and associated ages (Merle et al., 2009; Miranda et al., 2009); LVC, Lisbon Volcanic Complex; OCT, Ocean Continent Transition

the margin is also presented, taking into account the previously proposed presence of a deep seated (plume-like?) heat source and its repercussions on the maturation of regional prospective source rocks, and on how deformable plate paleogeographic models for hyper-extended margins evolve after breakup.

2 | GEOLOGICAL SETTING

Based on different geophysical datasets, including side scan sonar, single and multibeam bathymetry and seismic reflection data, the Estremadura Spur (Figure 1) corresponds to a major (200 km long and 90 km wide) E-W trending physiographic feature on the offshore of the West Iberia continental margin, consisting of a crustal block bounded by two major fault zones, the Nazaré Fault Zone (NFZ) to the north, and the Tagus Fault Zone (TFZ) to the south (e.g. Badagola, 2008; Pereira et al., 2017). Both fault zones have been interpreted as exerting a significant control on the tectono-stratigraphic evolution of the central domain of the margin and neighbouring basins (Alves et al., 2009; Pereira et al., 2017; Vanney & Mougenot, 1990). Along with other major fault zones inherited from the Palaeozoic Variscan orogeny, these first-order transcurrent zones were later reactivated during Jurassic to early Cretaceous continental extension, segmenting the margin into distinct basins, and ultimately localising deformation during the Alpine tectonic inversion of the margin (Alves et al., 2009; Pereira et al., 2017). Additionally, the Estremadura Spur is also part of a wider crustal lineament between the conjugate margins of Iberia-Newfoundland (Sibuet et al., 2007), and tied to the evolution of the Late Cretaceous alkaline magmatism in the Central Atlantic (Merle et al., 2019).

2.1 | Geodynamic evolution of the WIM

The rifted continental margin of West Iberia, located on the region between the Central and North Atlantic, records the prolonged effects of hyper-extension of the lithosphere, in which distinct segments shape its architecture (e.g. Manatschal & Bernoulli, 1999; Pereira et al., 2017; Sutra et al., 2013). During this process the WIM underwent multiphase rifting (Alves et al., 2009; Pereira & Alves, 2011), which initiated as part of the Late Triassic extension of Pangea and proceeded until the Early Cretaceous, when complete lithospheric breakup was achieved on the conjugate Iberia and Newfoundland margins (Bronner et al., 2011; Tucholke et al., 2007). Within this time frame, a total of four rift phases contributed to margin segmentation into discrete segments, bounded by inherited Palaeozoic first-order transfer zones that largely controlled its Meso-Cenozoic crustal architecture (Alves et al., 2009; Pereira et al., 2017). These distinct syn-rift phases are typified by unconformity bounded megasequences that build the larger framework of the conjugate margins, which include (Alves et al., 2009; Pereira & Alves, 2011 and references therein; Figure 2): (a) Late Triassic (Carnian?-Norian) to earliest Jurassic (Hettangian), initial extension and tectonic generalised subsidence, that accommodate continental deposits including alluvial-fluvial siliciclastics and evaporites; (b) Hettangian to Callovian, continued subsidence with punctuated regional uplift and erosion on the SW Iberian Margin, almost exclusively composed of marine carbonate sequences; (c) mid Oxfordian to Tithonian/Berriasian paroxysmal subsidence in SW Iberia and the Lusitanian Basin; and IV) Berriasian to Aptian/Albian, as a final phase of tectonic subsidence, mostly affecting the distal domains of the NW Iberian margin.

Lithospheric breakup on the WIM was ultimately achieved during the Aptian/Albian (Bronner et al., 2011; Tucholke et al., 2007), and resulted in the deposition of a distinctive depositional sedimentary package, the Lithospheric Breakup Sequence (LBS; Soares et al., 2012), in response to the cessation of rifting and significant sediment input (Figure 2).

Post-rift evolution of the WIM is predominantly characterised by thermal subsidence (Alves & Cunha, 2018; Stapel et al., 1996) and by infilling of the available accommodation, first by alluvial-fluvial siliciclastic deposits (Turonian-Santonian) and later by carbonate sequences denoting the progressive flooding of the margin, ultimately crosscut by a regional unconformity of Maastrichtian–Paleocene(?) age (Martín-Chivelet et al., 2019; Rey et al., 2006). The Tertiary is characterised by three megasequences comprising the Paleogene carbonates, overlain by Neogene and Quaternary dominantly clastic depositional units (GPEP, 1986; Pereira & Alves, 2012). Deposition throughout the margin was largely controlled by the effects of the Alpine orogenic cycle (progressive collision of Iberia with Eurasia and Africa), which on the WIM comprises three main tectonic events, namely (Cloetingh et al., 2002; Cunha, 2019; Mougenot, 1980; Mougenot et al., 1979; Ribeiro et al., 1990; Figure 2): (a) the Campanian?-Maastrichtian to Paleocene N-S phase; (b) the Eocene, broadly oriented on a NE-SW to N-S compression; and (c) the mid Miocene along a NW-SE shortening direction. These events resulted in significant erosion of the uplifted domains to the east and consequent sediment bypass towards the margin, along main NE-SW to WNW-ESE strike-slip controlled canyon incision (Alves et al., 2000, 2003; Pereira & Alves, 2013).

2.2 | The Late Cretaceous magmatic cycle

The WIM was the locus of substantial alkaline magmatic activity during the Late Cretaceous and contrasts both in

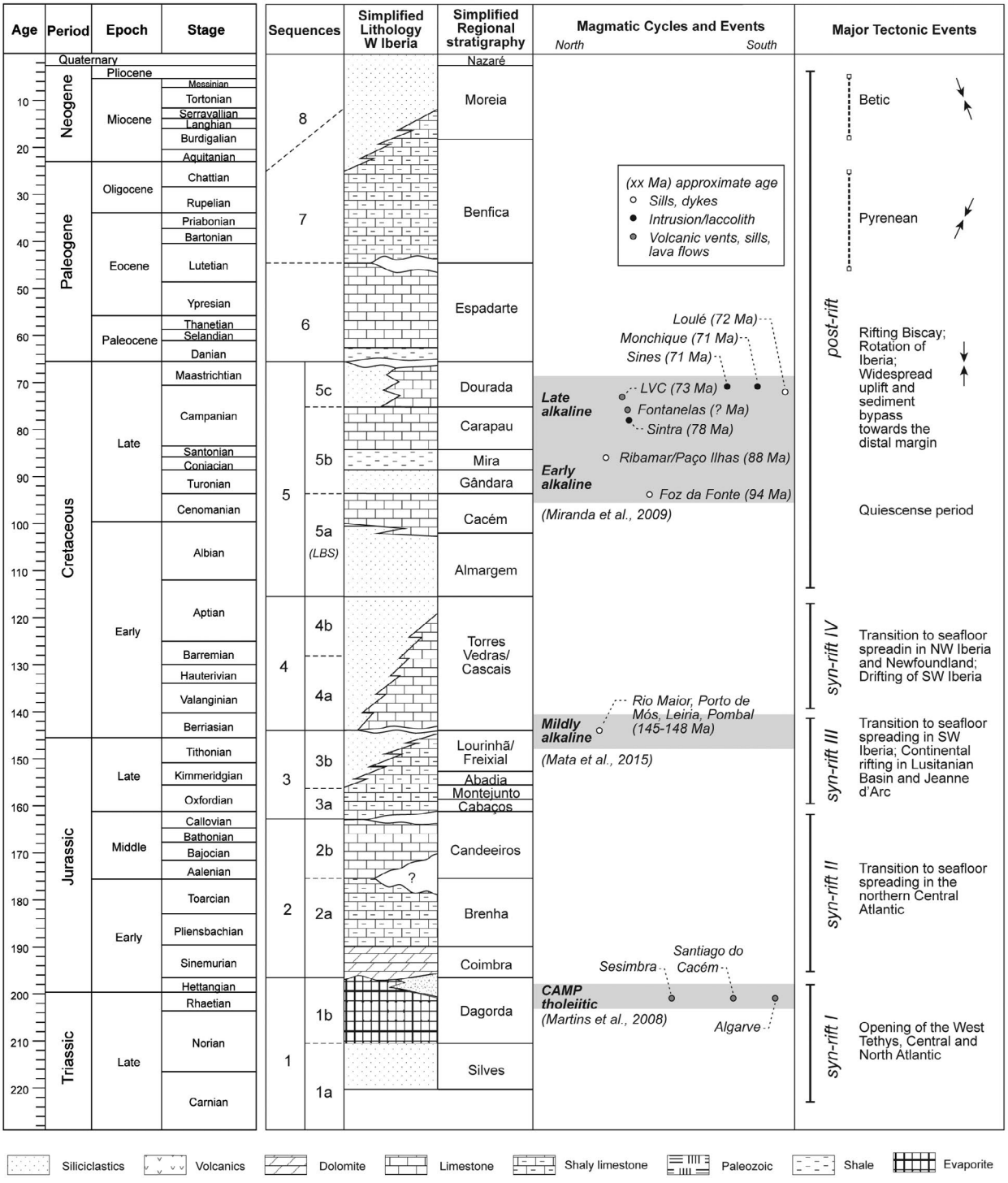

FIGURE 2 Simplified regional stratigraphy of the West Iberian Margin (modif. Pereira & Alves, 2012), associated magmatic cycles (Martins et al., 2008; Mata et al., 2015; Miranda et al., 2009) and major tectonic events controlling the evolution of the margin. LBS, Lithospheric Breakup Sequence

geographical distribution and geochemical nature from the previous syn-rift cycles (Mata et al., 2015 and references therein; Figure 2). The first cycle (ca. 200 Ma), part of the Central Atlantic Magmatic Province (CAMP), was tholeiitic in nature, with negative εNd_i and radiogenic initial Sr isotope ratios (>0.7050; Callegaro et al., 2014; Martins et al., 2008), whereas the second cycle (140–148 Ma) is mildly alkaline, showing $1.6 < \varepsilon Nd_i < 4.2$ and initial Sr isotope ratios close to the $CHUR_{145}$ (Grange et al., 2008; Mata et al., 2015). Conversely, the Late Cretaceous magmatism is characterised by $\varepsilon Nd_i > 5$ and initial Sr isotope ratios affine to a sub-lithospheric mantle source with a time-integrated evolution

characterised Rb/Sr ratios noticeably lower than the CHUR (Grange et al., 2010; Miranda et al., 2009).

Onshore, alkaline magma emplacement during the Late Cretaceous cycle occurred in necking to stretched domains of the otherwise thick continental crust, cropping out on three main sub-volcanic complexes: Sintra, Sines and Monchique (Miranda et al., 2009; Figure 1). Additional manifestations of the same magmatic cycle also included the eruptive Lisbon Volcanic Complex (LVC) and the hypabyssal/volcanic suites of the Algarve Basin, with ages ranging from 94 to 69 Ma (Grange et al., 2008, 2010; Miranda et al., 2009; Figures 1 and 2). On the offshore segments of the WIM, coeval alkaline magmatism is widespread, including on the Madeira-Tore Rise, although within a distinct oceanic crustal setting (Merle et al., 2009; Figure 1c).

Grange et al. (2010), based on the southwards decreasing age of the Sintra-Sines-Monchique subvolcanic massifs on the increasing alkalinity, $(^{206}Pb/^{204}Pb)_i$ and $(\varepsilon Hf)_I$, accompanied with a decrease in $^{87}Sr/^{86}Sr$, interpreted the expression of these magmatic intrusions as the result of the counter-clockwise rotation of the Iberia atop a sub-lithospheric stationary mantle plume (comprising distinct plume-lithosphere interactions, op. cit.).

The first insights into an offshore buried volcanic edifice, the Fontanelas Volcano, have been reported based on seafloor dredges that revealed geochemical affinities with the Late Cretaceous Alkaline cycle (Miranda et al., 2010), as well from combined gravimetric-magnetic and seismic datasets (Escada, 2019; Escada et al., 2019; Neres et al., 2018; Pereira et al., 2017; Pereira & Barreto, 2018; Silva et al., 2000; Simões et al., 2020).

3 | DATA AND METHODS

Investigating the multiple expressions of magmatism and its tectonic controls on the study area was accomplished by carrying out integrated seismic tectono-stratigraphic analysis and interpretation of distinct seismic-reflection datasets (Figure 1). Combined with numerous published references at onshore outcrops (e.g. Miranda et al., 2009; Ribeiro et al., 2013; Terrinha et al., 2017; Figure 2), in which the different characteristics of those igneous rocks constitute the comparative benchmark for investigating buried features offshore.

A regional analysis was performed using proprietary 2D multichannel migrated seismic reflection data in the time domain (acquired by TGS in 2000–2002 and FUGRO in 2008). In addition, exclusive high-resolution Pre-Stack Depth Migrated 3D seismic survey, acquired with 10 streamers with 8100 m cable length covering a full fold area of 2096 km^2 from CGG Veritas in 2010, with a shot point interval of 25 m. All seismic data were processed with zero phase and displayed with normal polarity following the standards of the Society of Exploration Geophysicists (SEG), where an increase in acoustic impedance corresponds to a positive reflection (red display on seismic) and a decrease in acoustic impedance (negative reflection) is displayed in black. Seismic resolution of the 3D dataset is variable for the interest intervals where magmatic features occur and for the key seismic stratigraphic intervals used for structural interpretation. Achieving an estimation of vertical resolution (e.g. Brown, 2011) points to low frequencies (5–15 Hz) at the area of a postulate intrusion with PSDM stacking velocities of around 5000–6000 m/s allowing to resolve features of 100–250 m, whereas for the areas where sills and a volcanic edifice is identified, frequencies range from 20–30 Hz with velocities of 3000–4000 m/s, resolution is around 25–35 m.

In the absence of direct well control or the lack of rock sampling and/or of isotopic dating of the offshore igneous rocks, constraining the age of the distinct magmatic features, their complying stratigraphic and structural setting, key stratigraphic markers were used to characterise in detail the main unconformity-bounded megasequences (sensu Hubbard et al., 1985), that allow applying a comprehensive seismic-stratigraphic framework (based on Alves et al., 2009; Pereira & Alves, 2011; Pereira et al., 2017), with linkage with the regional framework from the Lusitanian Basin (Azerêdo et al., 2003; Rey et al., 2006; Wilson, 1988; Witt, 1977; see Figure 2 and Table 1 for details). Identification of igneous features on the seismic profiles followed the criteria of Planke et al. (2015), for the identification and characterisation of sills, and Magee et al. (2013), for volcanic edifices. Recognition of the main faults in the area was accomplished by fully interpreting the 3D seismic dataset, applying multitrace variance attributes (a measure of waveform similarity for 3D seismic traces), that highlight the structuration of this segment of the margin, and ultimately by extracting its signal throughout rendered surfaces of meaningful seismic horizons.

4 | SEISMIC STRATIGRAPHIC CONSTRAINTS ON THE AGE OF MAGMATISM ON THE ESTREMADURA SPUR

Although the analysis of several gravimetric and geomagnetic studies have anticipated the occurrence of multiple magmatic features on the offshore WIM (Neres et al., 2018; Silva et al., 2000), a detailed seismic-stratigraphic analysis has not yet been achieved for most of these features. Recently, preliminary descriptions revealed the presence of a magmatic plumbing system in the ES, including multiple sills, dykes and a buried volcanic edifice (Pereira et al., 2017; Pereira & Barreto, 2018). Additionally, the first unequivocal evidence for a large intrusion in the Estremadura Spur (the so called

TABLE 1 Summary of the interpreted megasequences, their predominant seismic stratigraphic features, thickness and approximate ages

Megasequence	Top event	Criteria and internal features	Thickness (m)	Interpreted age of top event
8	seafloor	Subparallel to wavy horizons, locally downlapping; contourites; Incision surfaces	<500 m	Present day/Recent
7	Castillian to Betic inversion	Subparallel horizons, often downlapping; Mass Transport Deposits?	Locally eroded; 200–1200 m	Oligocene-mid Miocene (22-12? Ma)
6	Intra-Eocene; Pyrenean inversion	Subparallel horizons; Downlapping terminations; Mass Transport Deposits?	Locally eroded; 100–900 m	Mid Eocene (ca. 45 Ma)
5				
5c	Base Tertiary Unconformity; Rotation of Iberia	Subparallel horizons, medium to high amplitude; Top reflectors characterised by characterised by toplapping reflectors onto regional unconformity.	Locally eroded; 200–2200 m	Maastrichtian-Paleocene(?) (68-64? Ma)
5b	Onset of intrusion	Subparallel reflectors with low amplitude internal horizons; Basal units characterised by onlapping reflectors onto unconformity.	Locally eroded; 500–2800 m	Campanian (72–74 Ma)
5a	Lithospheric Breakup Sequence	Subparallel seismic reflectors with medium to high amplitude	Locally eroded. Typically, 300–400 m (up to 600 m)	Cenomanian (ca. 94 Ma)
4	End of Syn-Rift phase IV; Onset of seafloor spreading on NWIM	Limited growth strata, syn-rift deposits; medium to low resolution	Locally eroded. <1800 m	Aptian/Albian (ca. 120–112 Ma)
3	End of Syn-Rift Phase III	Growth strata; Often chaotic horizons	—	Tithonian-Berriasian
2	End of Syn-Rift phase II	Poor resolution	—	Late Callovian-mid Oxfordian
1	End of Syn-Rift phase I	Poor resolution	—	Rhaetian-Hettangian

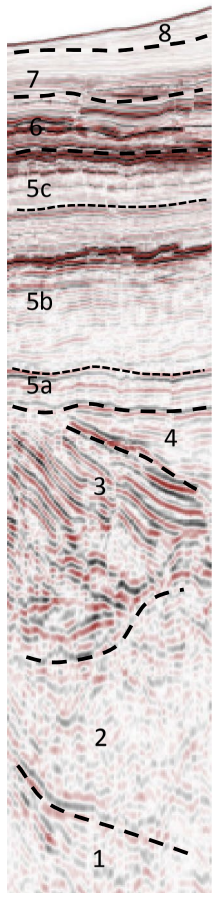

Estremadura Spur Intrusion, ESI), was established with the analysis of potential field data, which revealed that significant volumes of magma intruded and extruded in this specific domain of the WIM (Escada, 2019; Escada et al., 2019). Moreover in the absence of any age dating or boreholes intersecting any of these features, the timing of emplacement of these magmatic bodies was somewhat speculative and only established by comparison with similar events outcropping onshore.

Here, the description of the stratigraphic framework erected from seismic data is presented, from which the distinct depositional megasequences (Figure 2 and Table 1), allow a correlative estimation of the time period for the emplacement of these magmatic features.

4.1 | Syn-rift megasequences

Syn-rift strata are locally poorly imaged on the seismic record, especially in the western parts of the study area, where significant seismic noise is mainly due to the presence of the ESI (Figure 4 and Figure S2). Elsewhere, the syn-rift megasequences are characterised by diverging reflectors overlying an acoustic basement, with a total thickness up to 4000 m.

Megasequence 1 (see Table 1 for details), marks the onset of syn-rift deposition on the WIM during the Carnian(?)-Hettangian(?) interval, overlying a postulated Paleozoic acoustic basement. On outcrops and exploration wells (e.g. Azerêdo et al., 2003; GPEP, 1986; Witt, 1977), this megasequence is characterised by the accumulation of continental fluvial and alluvial strata (1a) and by an evaporitic unit (1b) that locally forms salt diapirs, exerting a strong control on the deposition and structural configuration of subsequent units (Figures 4 and 5).

Megasequence 2, of Sinemurian-Callovian age (Table 1), can be mainly interpreted on the eastern areas of the 3D survey, although limitations in imaging hamper the exact geometry and depositional nature of this segment of the margin. Despite these uncertainties, a depositional package can be broadly identified overlying the evaporitic unit and bounded at the top by an unconformity (Figure 4).

Megasequence 3 (mid Oxfordian-Tithonian/Berriasian) is characterised by fault bounded growth strata, typically thickening towards the east (Figures 4 and 5, Table 1), where major faults control the extension of the margin during the Late Jurassic third pulse of rifting. Although with limited resolution at depth on our datasets, these rift faults are apparently aligned along a N-S to NE-SW trend (e.g. Alves et al., 2002).

Megasequence 4 (Berriasian-Aptian; Table 1) is identified as a variable thickness unit (growth strata, with a total thickness up to 1800 m) onlapping the Late Jurassic strata, revealing the final events of rifting and associated tectonic subsidence throughout the WIM (Figures 4 and 5). The unconformity bounding the top of this megasequence (the breakup unconformity) is interpreted to mark the onset of seafloor spreading on the Iberia Abyssal Plain.

4.2 | Post-rift megasequences

Directly overlaying the breakup unconformity, Megasequence 5 is typically characterised by three subsets of distinct subparallel internal reflections (sequences 5a, 5b and 5c), each with specific aspects that allow further insights of the combined stratigraphic and magmatic events.

Sequence 5a, the basal sub-unit, is typified by the presence of subparallel reflectors that can be assigned to the LBS of Albian to Cenomanian age, as described in detail by Soares et al. (2012), which is a clear marker for establishing a solid tectonostratigraphic framework that in the present case permits constraining the age of magmatic events affecting the Estremadura Spur (Figures 4 and 5; Table 1). Similar to the descriptions by these authors for the northern WIM, this unit is characterised by continuous reflectors, blanketing the area of interest, with an overall thickness of 300–400 m, that locally can be as thick as 600 m. This seismic stratigraphic package marks the first depositional events subsequent to the onset of seafloor spreading.

Sequence 5b is characterised at the base by sub-parallel onlapping reflectors onto a noteworthy unconformity, showing an overall low to medium amplitudes. The reflection terminations observed can therefore be used as a seismic-stratigraphic marker that records a deformation pulse assigned to the folding of previously deposited strata and those sequences overlain on its flanks that are interpreted to mark the onset of an event that has affected the Estremadura Spur. It is within this unit that most of the evidence of a magma plumbing system is identified, with its descriptions presented in detail in the next section.

Sequence 5c reveals sub-parallel seismic reflections of medium to high amplitude, likely composed of carbonates (Figure 2). Downlaps are occasionally observed, although near the Fontanelas volcano seismic reflectors onlaps onto its flanks, thus allowing to narrow an approximate age for the extrusive event to the lower to mid-Campanian. This unit is truncated by a major and deformed unconformity interpreted as the Base Tertiary Unconformity (BTU) of Maastrichtian–Paleocene(?) age (Figures 3-6).

Overlying the BTU, three unconformity-bounded megasequences (Units 6, 7 and 8; see Figure 2 and Table 1) can be interpreted as marking the onset of Cenozoic infill of the margin. In some areas this whole depositional package can be as thick as 1500 m.

Megasequence 6 is characterised by strong amplitudes and subparallel reflectors typically downlapping the BTU, displaying significant thickness variations (up to 900 m; Figure 2 and

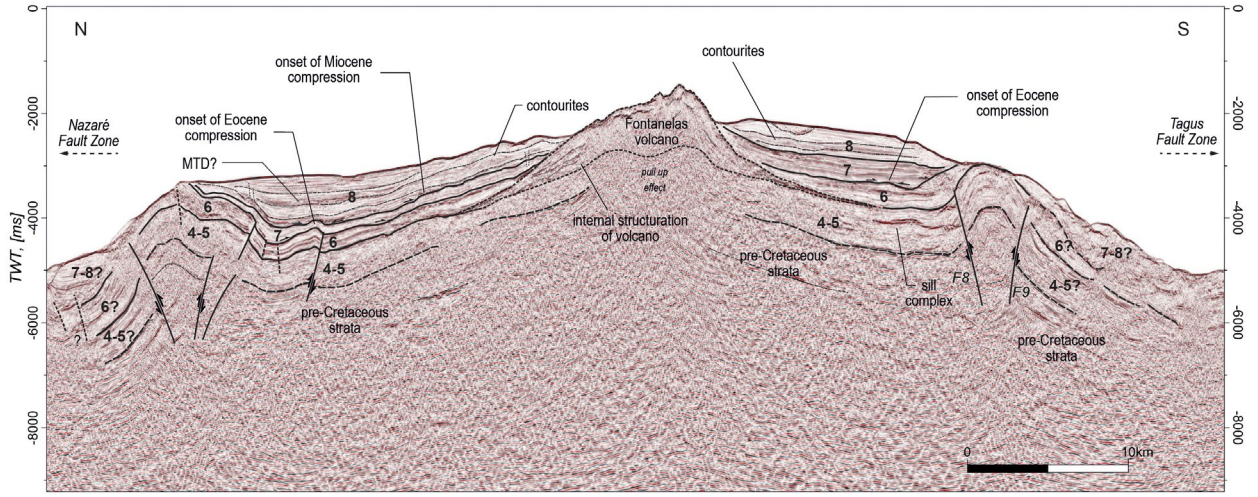

FIGURE 3 Regional seismic line (TWT) across the Estremadura Spur showing the Fontanelas volcano and evidence of post-rift margin inversion (see location in Figure 1b above). Numbers correspond to the regionally recognised seismotectonic megasequences in the WIM represented in Figure 2 above (see details in the main text)

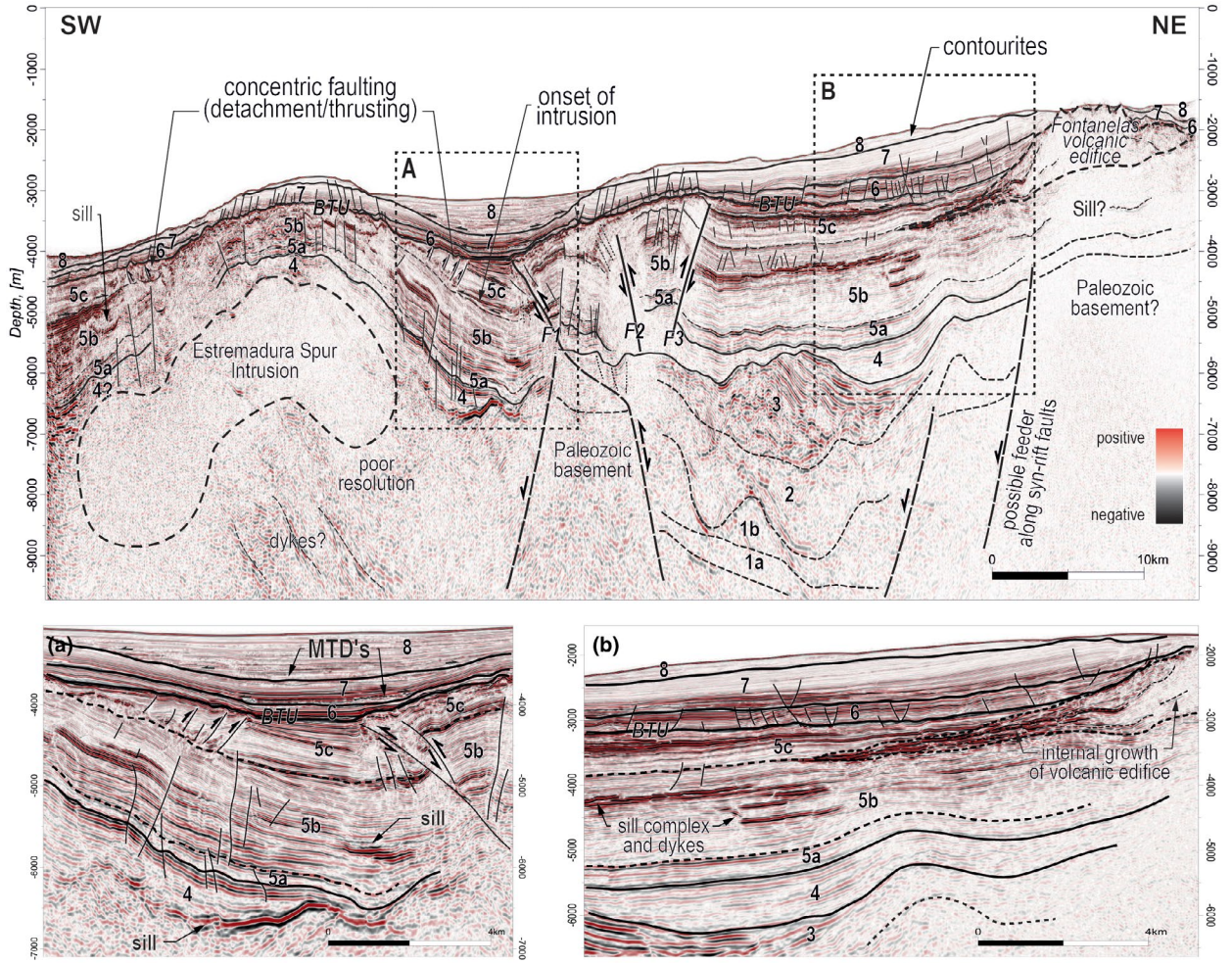

FIGURE 4 3D random seismic line (in depth) across the Fontanelas volcano, sill complexes and the Estremadura Spur Intrusion (see location in Figure 1b above), highlighting the distinct evidence of post-rift inversion. (a) Details of tectonic inversion features, igneous sills and Cenozoic deposition. (b). Details of sills complexes, the Fontanelas Volcano and post-BTU decoupled deformation. Numbers and legend as in Figure 2. BTU, Base Tertiary Unconformity; MTD's, Mass Transport Deposits

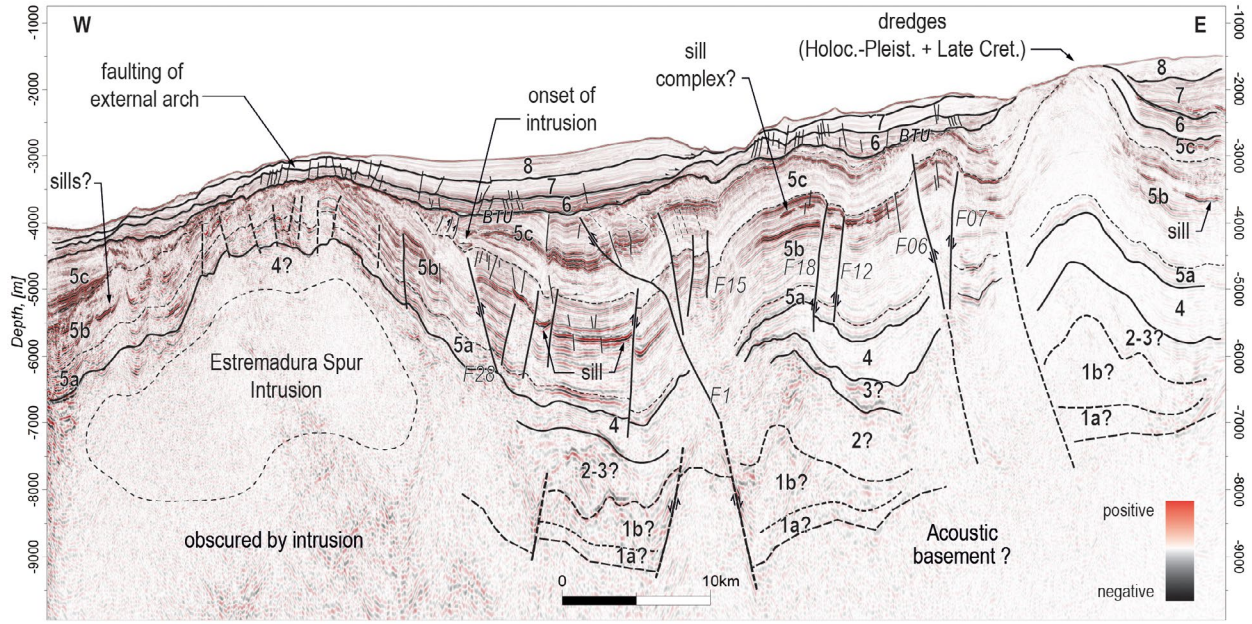

FIGURE 5 3D seismic line (in depth) across the Estremadura Spur (see location in Figure 1b above), showing distinct evidence of post-rift inversion. Numbers and legend as in Figure 2. BTU, Base Tertiary Unconformity

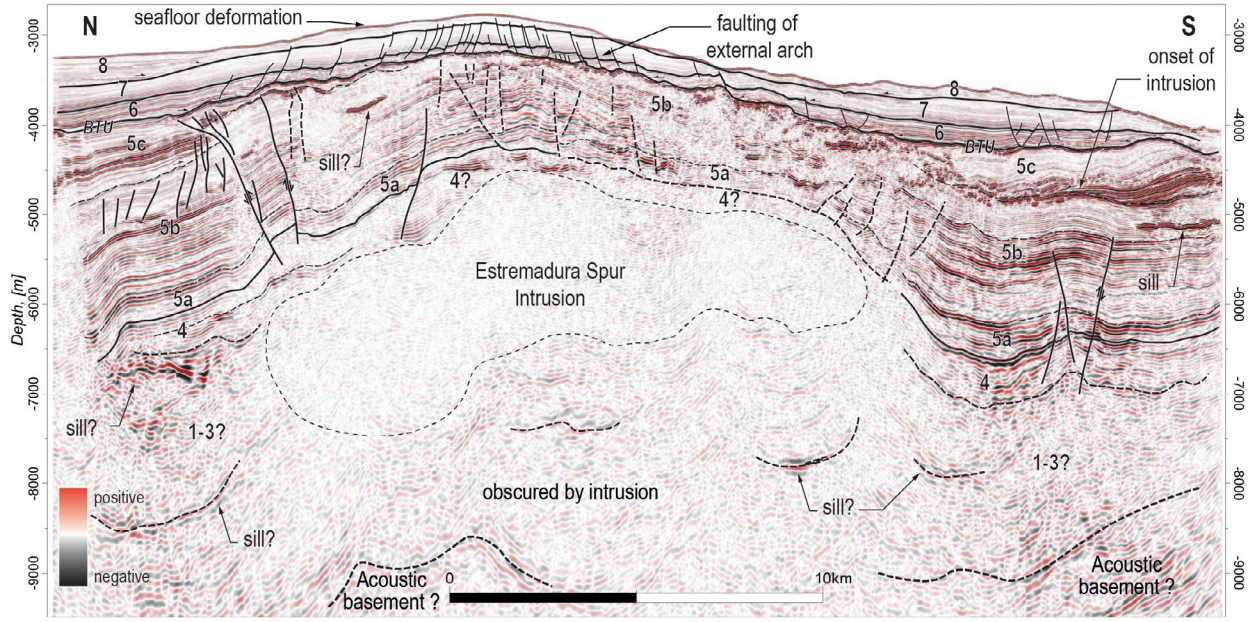

FIGURE 6 3D seismic line across the Estremadura Spur showing evidence of post-rift inversion. Numbers and legend as in Figure 2. BTU, Base Tertiary Unconformity

Table 1). The seismic-stratigraphic character of this unit, that is thin (or often absent) above growing anticlines, is interpreted as the expression of renewed deposition subsequent (and/or slightly simultaneous) to the several pulses of margin shortening and erosion (Figures 3-6), that bear proof of significant tectonic uplift associated with shortening pulses affecting the margin. In a trough NE of the ESI, chaotic reflectors can be observed at the base of Megasequence 6 (Figures 4 and 5), whose deposits can be interpreted to result from gravity-driven mass transport processes, associated to slope instability and rupture, in compliance with renewed uplift and significant erosion on the margin. Based on the information from outcrops, from onshore and offshore exploration boreholes, this unit is likely dominated by carbonate deposition with interbedded siliciclastic layers (e.g. Witt, 1977), and interpreted to represent the continuation of a similar Paleocene-mid Eocene mixed shallow marine depositional system (Figure 2).

Megasequence 7, of Eocene to Oligocene-mid Miocene(?) age, is dominantly characterised in the seismic record by layer-cake medium (to high) amplitude reflectors draping this segment

of the margin. These sequences are estimated to include marly to siliciclastic deposits (GPEP, 1986; Witt, 1977) that were accumulated with a maximum thickness of about 1200 m on the eastern areas of the survey (Figure 5 and Figure S3). However, at the base of this sequence, downlapping seismic reflectors often correspond to chaotic facies, likely representing downslope Mass-Transport Deposits (MTD; Figures 4-6 and Figure S4).

The uppermost depositional unit, Megasequence 8 (Oligocene-Miocene? to recent), onlaps a visible unconformity, often including incision surfaces and the evidence of chaotic reflections suggesting the presence of MTD's (Figures 4 and 5). Ultimately, these features are overlain by sub-parallel to wavy reflectors (contourites; see Llave et al., 2020), onlapping the flanks of growing anticlines, that point to significant amount of sediment bypass from the hinterland to the continental platform. In general, this unit has an observed variable thickness, with its main depocenters reaching a maximum of 450 m of sediment (Figures 3-6).

5 | EVIDENCE OF MAGMATISM ON THE ESTREMADURA SPUR

Late Cretaceous magmatism on the proximal WIM has long been the focus of numerous publications, mainly dedicated to the geochemical characterisation and petrological study of several known intrusive and extrusive complexes (e.g. Grange et al., 2010; Miranda et al., 2009; Rock, 1982). Less well known are the proposed offshore magmatic occurrences (Escada, 2019; Escada et al., 2019; Neres et al., 2014, 2018; Silva et al., 2000; Simões et al., 2020), for which a detailed imaging was still lacking. However, the absence of any absolute age determinations for any of these magmatic features hinders further conclusions on the exact timing of the corresponding volcanic event. Accordingly, the seismic stratigraphic analysis in this work, underpinned by the regional stratigraphic framework (Figure 2), has allowed constraining the age of such buried magmatic bodies. Indeed, these magmatic features post-date the LBS (top of sequence 5a, ca. 94 Ma), and are overlain by deposits from sequence 5c or crosscut by the BTU of Maastrichtian–Paleocene(?) age (Figures 3 and 4). This allows to broadly consider a Turonian(?)-Campanian age for the wider event, in agreement with the available geochronology constrains as summarised by Miranda et al. (2009) for the onshore occurrences (see Figure 2).

5.1 | The Fontanelas volcano

The Fontanelas volcanic edifice (Figure 1) is very well depicted on potential field data maps (Escada, 2019), as it is responsible for a free-air gravimetric anomaly exceeding 125 mGal and a total reduced to pole magnetic anomaly (International Geomagnetic Reference Field, IGRF removed) higher than 90 nT. Based on seismic data imaging, the volcanic edifice cropping out the seafloor (Figure 1) is interpreted to spread out over an area of about 350 km^2 (30 km long, 20 km wide), with an approximate height of 2500–3000 m from its base (Figures 3 and 4). Besides its triangular shape observed in seismic profiles, it can be identified based on the reflection terminations of strata onto its flanks and a high contrast of the seismic amplitudes at the top of its architecture. Internally, and similar to other examples from seismic profiling at New Zealand, South China and the North Atlantic (Bischoff et al., 2019; Planke et al., 2017; Sun et al., 2019; Walker et al., 2020), some discontinuous reflections indicate significant complexity that are likely to record the evolution and construction through time (Figures 3 and 4). At the base and flanks of the volcano, high amplitude seismic reflections suggest the preservation of lava flows, although their extent and detailed geometry are still unknown.

Constraints on the age of the extrusive event leading to the build-up of the volcanic edifice can be achieved by integrating this feature within the seismic-stratigraphic framework, as its base is positioned just below the top of sequence 5b. Conversely, the top of the volcano is overlain by multiple onlapping strata from sequence 5c, and ultimately by the Tertiary megasequences. This is an evidence that for a period of time, the volcanic edifice was exposed, either to a submarine or to sub-aerial conditions, although there is no clear evidence supporting which environmental conditions prevailed. Accordingly, a lower to mid-Campanian age is postulated for the Fontanelas volcano, suggesting that it may have preceded the installation of the onshore LVC (late Campanian, 74–71 Ma; Miranda et al., 2009).

5.2 | The Estremadura Spur Intrusion

Based on previous evidence from potential field data (Escada et al., 2019; Neres et al., 2014; Silva et al., 2000), a geophysical anomaly stands out on regional maps (Figure 1), that could either be assigned to an uplifted crustal block or the effect of an intrusive body, buried underneath Meso-Cenozoic sediments. However, the integration of gravimetric and magnetic data, presented by Escada (2019), unravelled the first detailed study of the extension, geometry and nature of the geophysical anomalies, that is broadly characterised by a free-air gravimetric anomaly in excess of 50 mGal and a total magnetic field (IGRF removed) over 90 nT, which, combined with the seismic dataset presented ahead, suggests that it is, in fact, an intrusive feature emplaced into the sedimentary strata.

Imaged on the western section of the 3D survey, this enigmatic feature is revealed as an acoustic feature characterised by its 'noisy' reflectors underlying a massive anticline, whose deposits are assigned to Megasequences 4 and 5a (Figures 4-6).

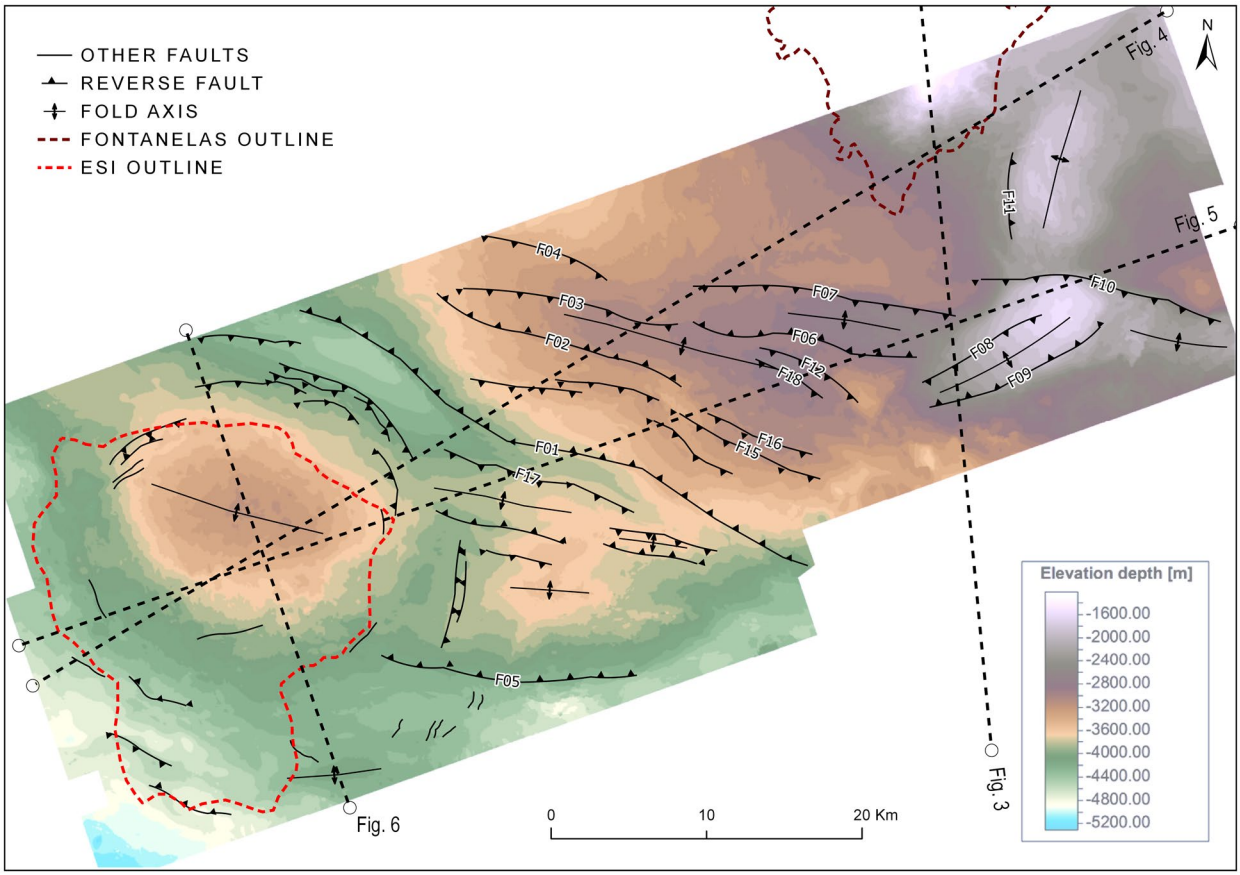

FIGURE 7 Structural base map of the Base Tertiary Unconformity (BTU; in depth), showing pre-Tertiary fault pattern

Syn-rift and early post-rift strata are strongly deformed in the area of the ESI, rendering the final geometry of the BTU surface at depth with a WNW-ESE elongated shape (Figure 7).

Here, the typical high amplitudes ascribed to the rheological contrast between an intrusive body and its surrounding strata (e.g. Planke et al., 2015) are not observed. This is possibly due to one or more of the following combined factors (all causing noise, signal absorption and significant less contrast): (a) intense faulting in the apex domain of the folded strata (outer arc region) atop the intrusive body; (b) contact metamorphism of country rock sediments; (c) technical limitations in seismic acquisition and/or data processing, such as unfitting stacking velocities.

Mapping the units above and beneath this feature led to the recognition of a N-S elongated body assigned to a laccolithic body (approximately 28 km long and 20 km wide), the ESI (Figures 6 and 7). This large laccolith bears an estimated total area of about 465 km^2, an average thickness slightly above 2000 m and an approximate rock volume of magma of 942 km^3. When compared with other documented laccoliths (e.g. offshore southern Australia, Jackson et al., 2013) the ESI shows some differences in its overall volume and shape, specifically regarding its pronounced aspect ratio (diameter/thickness = 14).

When visualised in cross-section (Figures 4-6), the folded strata overlying the ESI reveal a widespread bordering fault pattern that can be assigned to brittle accommodation of vertical (doming-like) inflation due to magma plumbing (see details ahead). This fault pattern, along with the overall shape and thickness of the intrusion, suggests that the ESI can be considered as a punched laccolith, which to some extent allow inferring on the brittle nature and cohesion of the host rock rheology (e.g. Schmiedel et al., 2017). The evidence for such a voluminous laccolith and the revealed level of detail on the deformation affecting associated (country rock) strata, is unique, not only on the WIM, but also in other passive margins worldwide.

Seismic stratigraphic criteria allowed to map in detail the onset of the intrusion, that is characterised by profuse onlapping onto a major unconformity, that in the area of the ESI is marked by these reflection terminations onto a growing anticline (base of unit 5c; Figures 4-6). Tentatively, a lower to mid-Campanian age can be considered as the most evident expression of the forced folding by magma emplacement, although some faulting of top sequence 5a in the ESI area may suggest some early structuration associated with the first events of plumbing at depth. Despite no isotopic age determinations were yet obtained for the ESI, the interpretation arising from

the seismic-stratigraphic data is consistent with the ages previously obtained for the onshore Sintra intrusive massif (Grange et al., 2010; Miranda et al., 2009), thus, supporting that the ESI is part of the same magmatic event. Accordingly, an estimated age of emplacement of the ESI can be assigned a period between the Turonian to the lower Campanian.

5.3 | Sills and sill complexes

Evidence of an important pre-Tertiary (below BTU) magmatic plumbing system, is preserved throughout the study area, mainly underneath and around the region of the Fontanelas Volcano, but also associated with the ESI. Evidence of such system is composed of multiple seismic features mainly observed dominantly within sequence 5b (Figures 4-6), thus suggesting an interpreted age for the emplacement of these features to have occurred during the Turonian-mid Campanian period (ca. 94–74 Ma). This estimated age is broadly synchronous with coeval sills cropping onshore, namely the Paço de Ilhas and Foz da Fonte described by Miranda et al. (2009).

The geometry of the sills is mainly characterised as planar to slightly saucer shape (Grange et al., 2010) and stand out on seismic, as high positive amplitudes at the top (and low negative amplitudes at the base), expressing a significant contrast in acoustic impedance with the surrounding sedimentary deposits (Figures 4-6). Locally, some sub-vertical inclined seismic features associated with these sill complexes are interpreted to represent dykes feeding the plumbing system (Figure 4b).

Additionally, associated with ESI, multiple high amplitude reflections are observed either underlying or overlying this laccolith-shape feature that are interpreted as sills (Figures 4-6). These are similar to those described by McLean et al. (2017) in the Faroe-Shetland Basin, and to the general setting of the outcropping Sintra intrusion in the WIM onshore associated with a complex of numerous radial and concentric dykes (Kullberg & Kullberg, 2000; Terrinha et al., 2017). However, those beneath the ESI and interpreted to intruding syn-rift deposits, lack the confidence in interpretation resulting from the limited resolution of the seismic dataset. These reveal a dissimilar geometry, as they appear as more concave saucer shape, when compared with those within sequence 5b, an aspect requiring further investigation on the possible geochemical nature of the magma and its rheological implications during emplacement.

6 | STRUCTURAL ANALYSIS

Subsequent to syn-rift extension and onset of seafloor spreading, the WIM underwent a period of relative tectonic quiescence (e.g. Cunha et al., 2009; Pereira & Alves, 2012; Stapel et al., 1996), dominated by the eastwards drifting of the Iberian microplate (e.g. Vissers & Meijer, 2012). However, the analysis of the subsurface on the western Estremadura Spur reveals complex structural patterns from the Cenomanian onwards (top sequence 5a), with noticeable evidence of post-rift tectono-magmatic interference. These aspects allow the characterisation of the processes through which shallow magma plumbing systems control structural strain accommodation in the vicinity of main intrusive bodies.

Post-rift deposits (of Late Cretaceous to recent age) record the multiple pulses of tectonic inversion materialised by conspicuous regional unconformities, folding and faulting. A comprehensive approach was achieved by mapping in detail the BTU, as this major unconformity depicts the broader post-rift structuration of the Estremadura Spur (Figure 7). Accordingly, three dominant styles of deformation are identified and described in detail, that include (Figures 3-6): (a) Deep seated reverse faulting and thrusting, driving some associated folding but without affecting the Tertiary; (b) Discrete local faulting associated with shallow magma emplacement during Late Cretaceous; and (c) Tertiary faulting decoupled from the underlying strata.

To characterise the distinct pulses of shortening and uplift of the margin, a series of variance maps were generated (Figures 8 and 9) that highlight the lateral discontinuities, which ultimately can be assigned to faulting within each megasequence. These include: (a) the layers associated with the early stages of seafloor spreading, the LBS (Sequence 5a; Figure 8a); (b) the onset of the intrusion of the ESI (Sequence 5b; Figure 8b); (c) the BTU (top of Sequence 5c; Figures 7 and 9a), as a major event that constrains the overall geometry of the area; and (d) the top Megasequence 6, a proxy for Neogene tectonic events (Figure 9b).

6.1 | Structuration during early post-rift

Fault F1 is the dominant feature in the area, extending over 40 km, crosscutting the entire syn-rift section and thrusting Late Cretaceous units towards the SW (Figures 4-7). This NW-SE thrust is interpreted to root at the pre-rift Palaeozoic units, which can be understood as a case of thick-skin tectonics similar to other examples, namely on the Southwest Iberian Margin (Pereira & Alves, 2013). F1 likely corresponds to an inherited syn-rift mechanical anisotropy that is interpreted to have worked early on as a normal fault during the multiphased rifting, successively reactivated with reverse kinematics during the several Cretaceous to Tertiary pulses of tectonic inversion (see Figure 4). Additionally, other shortening features include fault bounded anticlines, forming coeval NW-SE oriented pop-ups (e.g. F2-F3, F6-F7) and fewer others, approximately oriented NE-SW to NNE-SSW (F8, F9, F11; Figure 7).

The analysis of the variance seismic attribute within a 50 m depth window above the Cenomanian unconformity

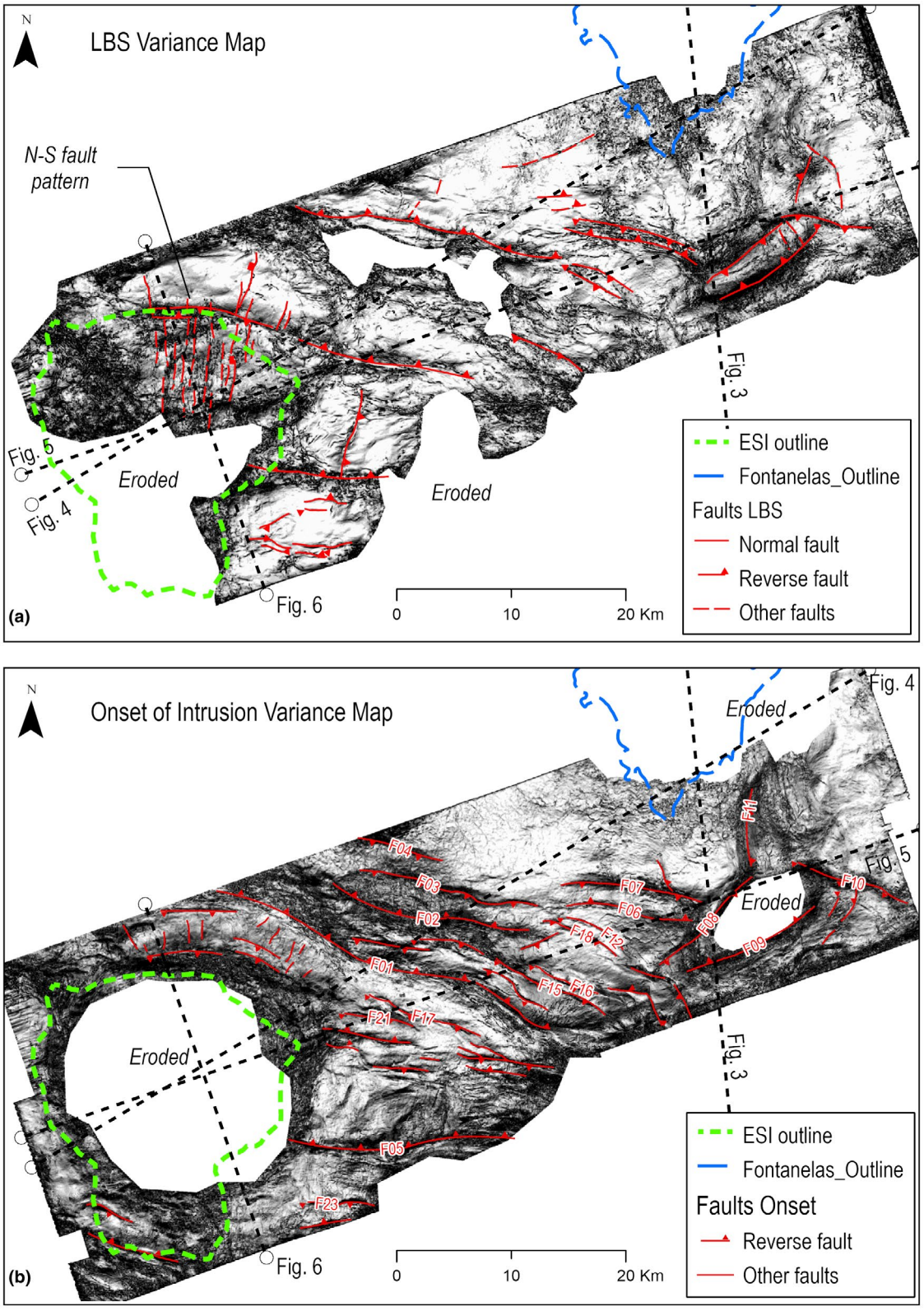

FIGURE 8 Variance attribute extraction highlighting the structural pattern of: (a) Top of sequence 5a (LBS – Lithosphere Breakup Sequence), on a 50 m window above the unconformity. Note the N-S normal faulting overlying the ESI; (b) Top of sequence 5c (Onset of ESI intrusion) with a 50 m window above the unconformity, showing the concentric fault pattern controlled by the emplacement of the ESI

reveals that Sequence 5a (LBS) is dominated by the pervasive NW-SE inversion features that represent the generalised shortening of the margin during the Tertiary (Figure 8a). However, a conspicuous N-S to NNE-SSW fault pattern materialises on the area of the ESI, characterised by normal faults at the crest of the intrusion. This group of faults are

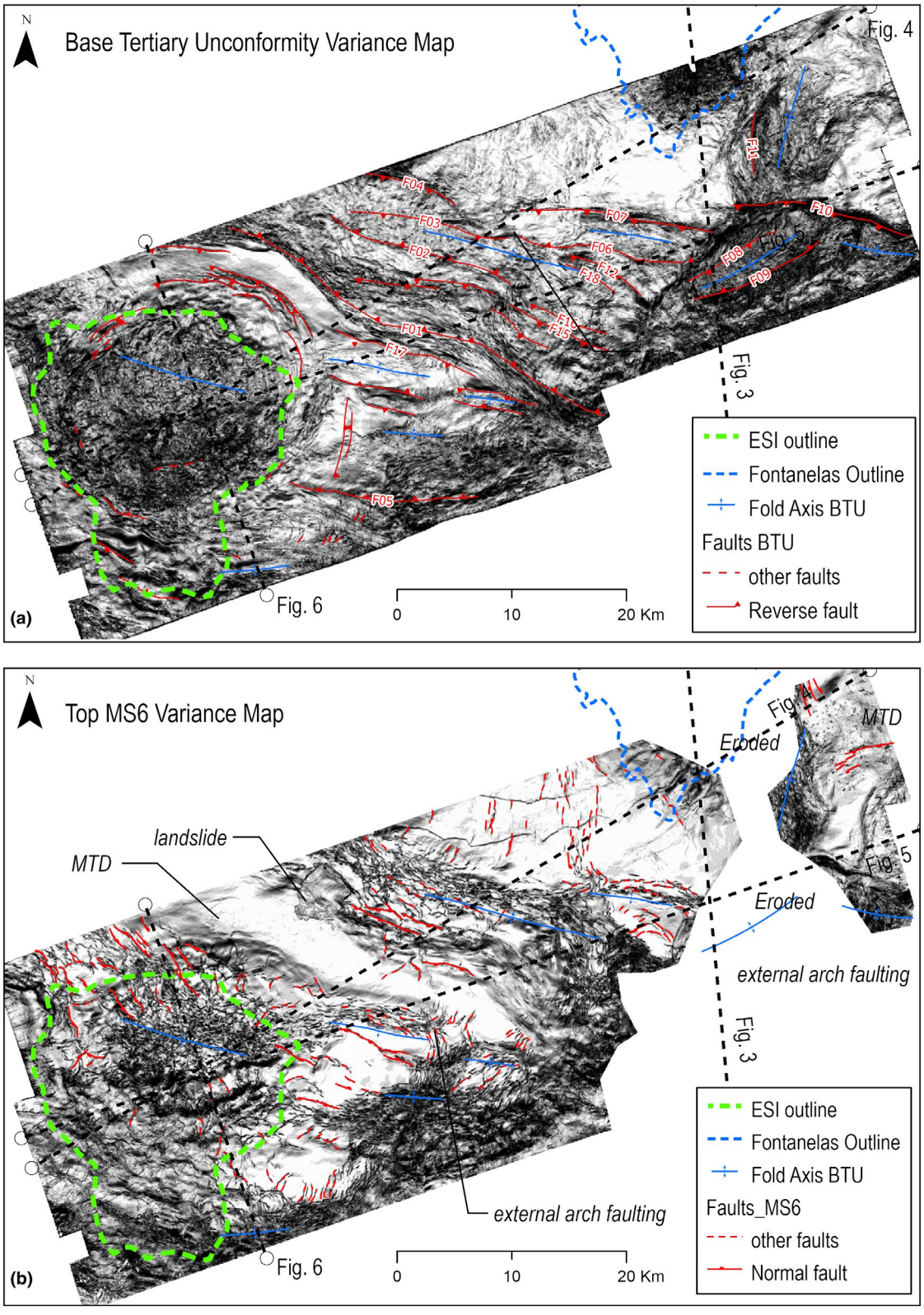

FIGURE 9 Variance attribute extraction highlighting the structural pattern of: (a) 50 m attribute below BTU, showing the major faults controlling the tectonic inversion; (b) 50 m above the top of Megasequence 6, highlighting the fault pattern associated with crestal deformation of underlying folding

interpreted to represent, either the accommodation of the earliest post-rift events associated with the immediate stress field during seafloor spreading along a broad E-W extension, or alternatively, the first evidence of magma emplacement at depth, with faulting due to extensional brittle accommodation in the outer arch of the overlying doming strata.

6.2 | Combined Late Cretaceous inversion and structural controls of associated magma plumbing systems

The opening of the Gulf of Biscay and the counter-clockwise rotation of the Iberia microplate (e.g. Vissers & Meijer, 2012) is described to have controlled the initial widespread shortening of the WIM accommodated by first-order transfer zones, which thus correspond to narrow domains of localised transpressive inversion (Pereira et al., 2017). This makes the Estremadura Spur a foremost region to investigate given the newly presented data, as it reveals the combined effects of earliest stages of margin shortening and deformation during magma ascent/emplacement.

The analysis of a variance map generated along a window of 50 m below the top Sequence 5b (Campanian unconformity), shows the effects of the predominant Late Cretaceous inversion and the subsequent imprint of the sustained Tertiary inversion (Figure 8b). At this stratigraphic level, the fault pattern is characterised by multiple reverse and thrust faults mainly oriented WNW-ESE verging towards the SW (e.g. F1, F2), although some approximately SW-NE reverse faults can be identified at the eastern part of the survey (e.g. F8 and F9), as well as SSW-NNE reverse fault-bounded anticlines.

In the close vicinity of the intrusion, a group of concentric reverse faults is rooted at the intra-Campanian unconformity and mostly aligned with the NW-SE anticline axis (Figure 8b; Figures 4 and 5). These faults are interpreted to have acted as shortening features on top of a detachment layer during the combined tectonic inversion and magma emplacement (Figure 4a). This alignment of reverse faulting suggests a NE vergence, an aspect that can be associated with the Late Cretaceous final stages of ascent and emplacement of the laccolith. Note that these reverse faults do not propagate above the BTU, thus allowing to determine that they were active only for a short period of time associated with the period of forced folding caused by the emplacement of the ESI laccolith.

Sequence 5c is eroded at the crest of the ESI, locally truncated by the BTU and often cropping out at the seafloor (Figures 4-6), showing that folding forced by magma emplacement controlled significant localised uplift and the depositional response of coeval strata at the flanks of the growing anticlines (Figure 9a). The asymmetric ring fault pattern around the ESI closely resembles analogue modelling results of forced folding and doming processes at shallow crustal levels (Montanari et al., 2017; Roman-Berdiel et al., 1995). Considering that these ring faults are mainly located close to the NE limit of the ESI, this is interpreted as a possible predominant direction of magma ascent, determining asymmetric strain localisation by forced folding on the NE limb of the growing anticline (Figure 9a).

6.3 | Tertiary inversion

The Cretaceous-Tertiary transition is marked by a regional unconformity (BTU; Figure 7), that can be recognised throughout the WIM, as it defines a period of significant uplift/tilting of the proximal margin, resulting in noticeable sediment bypass from the hinterland towards the marine Atlantic domain (Alves et al., 2003; Cunha, 2019; Pereira & Alves, 2013). On the Estremadura Spur, the geometry of the BTU is characterised by its intensively folded geometry (Figure 7), mimicking the underlying structuration where reactivation of the Late Cretaceous reverse faults and folds accommodates persistent margin shortening during the Tertiary (Figures 4-6).

Brittle deformation below and above the BTU is noticeably dissimilar denoting the decoupled character of the deformation that is characterised by the non-propagation of major faults into the Tertiary (Figures 8 and 9). Fittingly, the fault pattern observed on variance map of top Megasequence 6, a proxy to Tertiary inversion is characterised by normal faulting crosscutting to Megasequence 7, although decoupled from the underlying Late Cretaceous inversion structures (Figure 9b). The fault pattern affecting these Eocene-Oligocene sequences show distinct predominant directions, depending on their location and underlying controls, that include: (a) a group of normal faults identified in the area of the ESI, characterised by an overall radial pattern; (b) a family of NW-SE oriented normal faults with limited throw associated with the crest of growing anticlines at depth and, (c) some N-S normal faults located southwest of the Fontanelas Volcano.

Megasequence 8 (mid Miocene to recent) does not show significant faulting, contrasting with the deformation affecting MS7. This aspect suggests that during this period tectonic activity is significantly decreased and that the controlling mechanisms would likely be associated with some minor tilting of the margin as a whole, as evidenced by the westwards inclined character of seismic horizons.

7 | DISCUSSION

In the studied Estremadura Spur transcurrent domain of the extended continental WIM, the collected magmatic-tectono-stratigraphic data reported above has revealed the prevalence of decoupled deformation affecting syn-rift units, post-rift strata, and the Tertiary sedimentary cover (Figure 10). This unveils a scenario of interference between regional multiphased tectonic-inversion events and localised effects of magma emplacement associated with major intrusions at depth.

The interplay of both margin shortening and magma emplacement resulted in a tectono-magmatic overprinting pattern, whose interpretation allows clarification of the role of

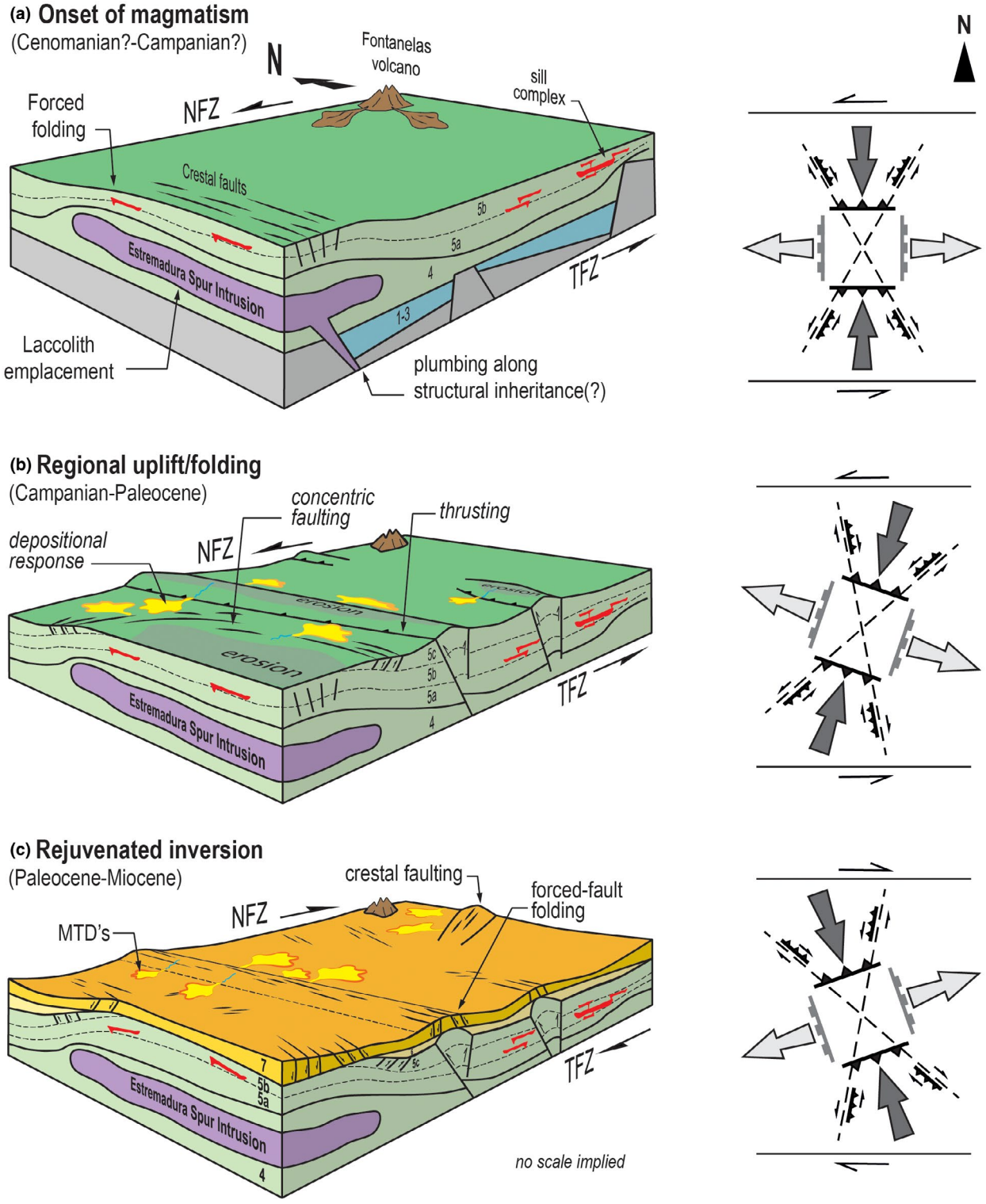

FIGURE 10 Schematic block-diagram illustrating the main phases of inversion and the combined evidence of a magma plumbing system on the Estremadura Spur. MTD, Mass Transport Deposits. (a) Structuration during the onset of inversion and magmatism. (b) Period of intense deformation during the latest Cretaceous showing preferred areas and styles of inversion. (c) Rejuvenated period of margin shortening, with deformation decoupled from undelying Cretaceous strata

first-order transfer zones in localising regional (large-scale) deformation at specific segments of the WIM. More generally, it also provides unprecedent new insight on the role of sub-lithospheric mantle sourced magma pulses in the evolution of passive continental margins evolving under similar conditions.

7.1 | Strain decoupling during magma plumbing and tectonic inversion

The evolution of the passive continental margin of West Iberia was largely controlled by post-rift inversion (Cloetingh et al., 2002; Mougenot et al., 1979; Ribeiro et al., 1990). This process resulted in focused shortening along deep rooted faults, some of them inherited from the Variscan orogeny and subsequently rejuvenated during rifting (e.g., MPFZ and the NFZ; Pereira & Alves, 2013; Pereira et al., 2017), acting as sharp transfer zones between adjacent alternating crustal segments (lower to upper plate architecture; Pereira et al., 2017; Péron-Pinvidic et al., 2015).

Subsequent to lithospheric breakup, tectonic efforts are recorded on the ES, reflected by a N-S fault pattern crosscutting the LBS (Figure 10a), interpreted to represent the early evidence of magma emplacement at depth of the ESI, during the Cenomanian-Campanian(?). Onshore, the Foz da Fonte sill (dated ca. 94 M.a., Miranda et al., 2009), may be coeval to the onset of magmatism of the ESI. However, hindered by limited seismic data resolution the absence of any age dating of the magmatic features in the area, such aspects still require further investigation.

During Late Cretaceous to Tertiary inversion three major inversion events shaped the margin, namely: 1) the Campanian-Maastrichtian, 2) the Paleocene-mid Eocene, and 3) the Oligo-Miocene. These events, combined with the emplacement of magma, created an interference pattern of folds and faults that allow explaining how specific segments of passive margins can accommodate stresses in the presence of rigid bodies within the sedimentary succession.

Multiphased inversion on the ES resulted in a series of predominantly NW-SE and NE-SW fault-propagation folds verging respectively to SW (e.g. F1, F6) or to the NW (F8; Figures 3-6). This work reveals that, largely controlled by the counter-clockwise rotation of Iberia driven by rifting on the Bay of Biscay and onset of the collision in the Pyrenees (Vissers & Meijer, 2012), the initial shortening event (Campanian-Maastrichtian), is the most expressive in terms of the magnitude of deformation. These NW-SE faults are far more significant and important than the latter, in compliance with significant margin inversion under a Late Cretaceous left-lateral transpressive regime, prior to Tertiary reactivation (Figure 10b). By analysing the different post-rift strata, it becomes patent that sequence 5C accommodates most of the inversion, as evidenced by significant thickness variations and noteworthy truncation due to erosion along the BTU (Figures 3-6). It remains to be clarified whether the NW-SE fault-propagation folds and pop-ups are synchronous with those aligned SW-NE (Figures 8 and 9), although data may suggest that these later features are younger and likely associated with a different pulse of inversion.

This tectonic event was coeval with the ascent of fertile mantle sourced magma plumes (Merle et al., 2019; Miranda et al., 2009) that resulted in the installation of a laccolith (ESI), associated sill complexes and early manifestations of extrusive magmatism precursor of the Fontanelas Volcano. The combined tectono-magmatic interaction between these two processes resulted in the generalised forced folding and reverse faulting (Figures 4-7), associated with the emplacement of the ESI that has created a localised family of concentric faults (Figure 8). Comparable fault patterns interpreted to control magma flow intrusive paths have been previously reported by sandbox analogue modelling studies (Montanari et al., 2017), although subsequent events of strike-slip inversion were also shown to overprint the final stress patterns and implied fault configurations (Corti et al., 2005; Gomes et al., 2019; Figure 10). To some extent, such interferences correlate well with the observed increasing deformation of overburden strata at the (onshore) outcropping Sintra and Sines massifs, that show their respective northern flanks affected by significant folding and south-dipping bounding faults (Inverno et al., 1993; Kullberg & Kullberg, 2000).

The second shortening event (Paleocene-mid Eocene) is generally ascribed to the large-scale NE-SW collision of Iberia with the Pyrenees and resulted in the reworking of the inherited Late Cretaceous fabric (Figure 10). Such a reactivation consisted mainly in fault-propagation folding, deforming (but not faulting) the BTU, and in the associated depositional response recorded by the onlapping reflections within Megasequence 6 (Figures 4-7). Evidence of significant Eocene compression is still unclear on the onshore domains of the margin, although on the immerse regions of the continental platform such compression seems more significant (Boillot et al., 1979; Mougenot et al., 1979; Pereira et al., 2011), likely facilitated by the weaker rift-related rheology of the thinned continental crust.

A third event of deformation occurred on the ES (Oligocene-Miocene), noticeably different from the preceding ones, typified by the distinct direction of compressive stresses and the expression of fault patterns, highlighting the decoupled nature of deformation in between megasequences (Figure 10b-c). This period is characterised by continued buckling and associated localised normal faulting dominantly focused on the external arches of existing anticlines (faulting of Megasequence 7, Figure 9b). The associated depositional response consisted in the formation of mass flow deposits and sediment bypass towards the oceanic domain (Figure 10c).

Overall, the evidence of distinct fault patterns during the different phases of combined tectono-magmatic interplay and their associated controls reflects the changing directions of the stress fields as they rotate from a N-S during the Late Cretaceous, to a NE-SW trend during the Maastrichtian-Paleocene interval and ultimately, towards a NW-SE shortening event, from the Eocene onwards (Figure 10).

Aiming to clarify the role of the magma mechanical behaviour in the area, as well as any kinematic indicators associated with the geometry of the ESI and overlying strata, the changing rheology of the intrusion must be

accounted for at the distinct stages of inversion. As such, a viscous behaviour for the ESI is considered to have been determined by the Late Cretaceous magma ascension and emplacement, as evidenced both by the oblate and irregular geometry of the N-S aligned laccolith, and by the forcing concentric faults towards the NE. As simulated in several analogue modelling studies (Corti et al., 2005; Gomes et al., 2019), the deformed geometry of the ESI suggests that this magmatic body must have endured significant syn-tectonic shearing in a non-rigid state.

However, the analysis of the anticlines and their fold axis mapped on the BTU and top Megasequence 6 (dominantly oriented WNW-ESE, Figures 7 and 9) suggest a change in the orientation of the compressive stress fields during the Tertiary in compliance with a change in their main trend from a NE to a NW oriented direction. This bears implications for the accommodation of stresses on the ESI, which by this time would have achieved a rigid state, while the deformation in the overburden would still be accommodated in a ductile manner, through folding, under a dominant right-lateral strike-slip regime determined by the bounding first-order transfer zones. Although limited by the dataset extent, the major fault trends adjoining the ESI for the Tertiary successions, suggest a σ-type sigmoid generated under a right-lateral strike-slip, a feature concurrent with the general NFZ-TFZ interpreted displacement during the rotation of Iberia (Figure 10).

8 | CRUSTAL INHERITANCE CONTROLS FOR MAGMA PLUMBING SYSTEMS

Magma ascent and emplacement a typically controlled by pre-existing structural fabrics, with multiple examples described from passive margins worldwide and sandbox models, often under transtensive settings (Breitkreuz & Mock, 2004; Dini et al., 2008; Roman-Berdiel et al., 1995).

On the WIM, and more specifically on the onshore Lusitanian Basin, examples of inherited structural controls are reported for all the three Mesozoic magmatic cycles, for example, the 600 km long Messejana tholeiitic dyke (Cebriá et al., 2003), the mildly alkaline dykes from the Late Jurassic-early Cretaceous magmatic cycle (e.g. Mata et al., 2015) and for the alkaline magmatism with widespread evidence during Late Cretaceous (e.g. Lisbon Volcanic complex, the radial cone-sheet dyke complex; Kullberg & Kullberg, 2000; Terrinha et al., 2017).

The Estremadura Spur, a segment controlled by major bounding strike-slip zones, is a preferred location to assess the role of structural inheritance in conditioning specific post-rift inversion, as well as the combined effects of magma ascent/emplacement at a shallow crustal level. However, the exact contribution from syn-rift structural fabrics is still unclear, with seismic resolution hampering further evidence on how preponderant extensional faults may have controlled magma ascent and emplacement. Nonetheless, alike the well-known nearby examples of the Sintra laccolith (Terrinha et al., 2017) and of the Arrábida mountain chain (Kullberg et al., 2006), the presence of deeply rooted transfer zones seems to have played a role in favouring magmatic intrusions at shallow crustal levels in domains of hyper-extended continental crust.

The inherited hinge zone bounded by the NFZ and the TFZ (Figure 3 and Figure S1) denote significant focused shortening dominated by the changing stress fields from Late Cretaceous to mid-Miocene inversion pulses, resulting in SW verging reverse faults and anticlines. This, associated with the interpreted elliptical W-E shape of the ESI, suggests an inversion under right-lateral transpressive regime during the Tertiary (Figure 10c), with the ESI now acting as a rigid body with surrounding strata accommodating significant deformation in the area (Figures 8 and 9).

The recorded tectono-stratigraphic evolution points to a large-scale scenario, in which adjacent WIM domains, separated by major bounding transcurrent corridors, might accommodate differently the same compressive stress implied by the overall tectonic inversion of the margin.

8.1 | Implications for fluid flow and thermal regime

Acknowledging the wider extension and importance of the Late Cretaceous alkaline magmatic cycle on the margin, the impact to intra-sedimentary fluid flow and local thermal regime needs to be re-assessed, as these evidences bear implications for the potential presence of hydrocarbon occurrences.

Typically, petroleum systems modelling on the WIM account for either one or two heat flow events, respectively for the Early and Upper Jurassic (*ca*. 200 and 150 Ma) coincidentally with the two first Mesozoic magmatic cycles at the WIM. A third flow event has been also invoked, associated with the early Cretaceous extension (Casacão, 2015; Teixeira, 2012), but not including the 100–70 Ma period of significant mantle to crust magma and heat transfer on the Iberia Atlantic Margin. Accounting for a likely heat flow event during the Late Cretaceous may bear impact on the modelling of prospective petroleum systems on the WIM, in which some models cannot predict mature hydrocarbons without the help of an additional thermal event that would bring a speculative oil kitchen to maturity stages (Teixeira, 2012).

Additionally, the presence of a widespread thermal event on the central and southwest Iberian margin, in the area of influence of a mantle plume during this period is likely to induce noticeable fluid flow (e.g. Holford et al., 2017), that could react with carbonate depositional sequences, resulting

in the modification of the rheological properties of the extended continental margin and favour preferred zones for inversion and margin shortening.

9 | CONCLUSIONS

Based on high resolution 2D/3D multichannel seismic surveys from central West Iberian Margin (Estremadura Spur), this work documents the combined effects of sub-lithospheric post-rift magma plumbing system and tectonic inversion from Late Cretaceous onwards, showing the evidence of four major post-lithospheric breakup tectono-stratigraphic events largely controlled by the rotation of Iberia during the Alpine cycle.

The first tectonic event is assigned to the Turonian-Campanian, that marks the onset of magmatism, resulting in the localised bulging of strata with N-S extensional faults atop of a sizeable laccolith (the Estremadura Spur Intrusion) coeval with the emplacement of multiple sill-complexes and the formation of a volcanic edifice. The second event, of Campanian–Maastrichtian age, is not only associated with significant margin shortening, accommodated through multiple reverse faults and folding dominantly verging towards the SW, but also by the magma induced forced folding and concentric faulting of the latest Cretaceous strata. All sequences are ultimately locally crosscut by a regional unconformity of Maastrichtian–Paleocene(?) age, thus indicating that the Late Cretaceous inversion is far more significant than anticipated. However, the deep-rooted reverse faults from the Late Cretaceous (some inherited from the syn-rift extension), do not propagate to the Tertiary indicating that rupture at depth is sealed below the Base Tertiary Unconformity. During the Paleocene-mid Eocene, shortening and inversion resume, by re-adjusting to the new stress field direction (NW-SE), mainly by tilting of the margin and associated depositional response infilling, recorded by new space accommodation onlapping onto growing anticlines. The final stage of margin shortening (Oligocene-mid Miocene) is characterised by rejuvenated inversion, dominated by crestal faulting on the hinges of growing anticlines, reinforcing the decoupled nature of strain accommodation with depth. This event is accompanied by the depositional response bearing MTD's and onset of canyon incision.

Additionally, the detailed analysis of the Estremadura Spur Intrusion (a laccolith with approximately 942 km^3), suggests that its emplacement is controlled by the presence of syn-rift inherited faults and that later, during inversion, this feature acted as a rigid body that accommodated discrete Tertiary dextral transpressive stresses by inducing faults which form a sigmoidal geometry at overburden level.

Ultimately, this tectono-magmatic interplay bears implications on how future analysis on the rheology of thinned continental crust evolves under the influence of combined transpressive stresses and how, as part of a wider magmatic province, heat transfer from such intrusive bodies can be reflected on thermal models assessing organic maturity of similar post-extensional magma-poor rifted margins.

ACKNOWLEDGEMENTS

Authors wish to acknowledge the treasured contribution of Prof. Fernando Monteiro Santos, from the Dept. Engenharia Geográfica, Geofísica e Energia, Faculdade de Ciências da Universidade de Lisboa, for the fruitful discussions and contributions to the project. We also kindly acknowledge the support of Partex Oil and Gas for supporting this research and by allowing to publish selected elements of the seismic dataset. We additionally acknowledge the financial FCT support through project UIDB/50019/2020 – IDL.

CONFLICT OF INTEREST

The authors declare that there is no conflict of interests.

PEER REVIEW

The peer review history for this article is available at https://publons.com/publon/10.1111/bre.12524.

DATA AVAILABILITY STATEMENT

The data that support the findings of this study are available from the corresponding author upon reasonable request. The data that support the findings of this study are provided in the supplementary material. The data that support the findings of this study are available from a third party. Restrictions apply to the availability of these data, which were used under license for this study.

ORCID

Ricardo Pereira https://orcid.org/0000-0003-4589-1145
Filipe Rosas https://orcid.org/0000-0002-6734-2916
João Mata https://orcid.org/0000-0001-5769-7708
Patrícia Represas https://orcid.org/0000-0002-2987-2836

REFERENCES

Alves, T. M., & Abreu Cunha, T. (2018). A phase of transient subsidence, sediment bypass and deposition of regressive-transgressive cycles during the breakup of Iberia and Newfoundland. *Earth and Planetary Science Letters*, *484*, 168–183. https://doi.org/10.1016/j.epsl.2017.11.054

Alves, T. M., Gawthorpe, R. L., Hunt, D., & Monteiro, J. H. (2000). Tertiary evolution of the são vicente and setúbal submarine canyons, southwest Portugal: insights from seismic stratigraphy. *Ciências Da Terra*, *14*, 243–256.

Alves, T. M., Gawthorpe, R. L., Hunt, D. W., & Monteiro, J. H. (2002). Jurassic tectono-sedimentary evolution of the northern Lusitanian basin (Offshore Portugal). *Marine and Petroleum Geology*, *19*, 727–754. https://doi.org/10.1016/S0264-8172(02)00036-3

Alves, T. M., Gawthorpe, R. L., Hunt, D. W., & Monteiro, J. H. (2003). Cenozoic tectono-sedimentary evolution of the western Iberian margin. *Marine Geology*, *195*, 75–108. https://doi.org/10.1016/S0025-3227(02)00683-7

Alves, T. M., Moita, C., Cunha, T., Ullnaess, M., Myklebust, R., Monteiro, J. H., & Manupella, G. (2009). Diachronous evolution of late Jurassic-cretaceous continental rifting in the Northeast Atlantic (West Iberian Margin). *Tectonics*, *28*(4). https://doi.org/10.1029/2008tc002337

Azerêdo, A. C., Duarte, L. V., Henriques, M. H., Manupella, G., & (2003). *Da Dinâmica Continental No Triásico Aos Mares Do Jurássico Inferior E Médio* (p. 43). Lisbon, Portugal: Instituto Geológico e Mineiro.

Badagola, A. (2008). *Evolução Morfo-Tectónica Da Plataforma Continental Do Esporão Da Estremadura*. Universidade de Lisboa.

Bischoff, A., Nicol, A., Cole, J., & Gravley, D. (2019). Stratigraphy of architectural elements of a buried monogenetic volcanic system. *Open Geosciences*, *11*(1), 581–616. https://doi.org/10.1515/geo-2019-0048

Boillot, G., Malod, J. A., & Mougenot, D. (1979). Évolution Géologique De La Marge Ouest-Ibérique. *Ciências Da Terra*, *5*, 215–222.

Breitkreuz, C., & Mock, A. (2004). Are Laccolith complexes characteristic of transtensional basin systems? Examples from the permo-carboniferous of central Europe. *Geological Society, London, Special Publications*, *234*, 13–31. https://doi.org/10.1144/GSL.SP.2004.234.01.03

Bronner, A., Sauter, D., Manatschal, G., Péron-Pinvidic, G., & Munschy, M. (2011). Magmatic breakup as an explanation for magnetic anomalies at magma-poor rifted margins. *Nature Geoscience*, *4*, 549–553. https://doi.org/10.1038/ngeo1201

Brown, A. R. (2011). *Interpretation of three-dimensional seismic data* (p. 534). AAPG SEG.

Callegaro, S., Rapaille, C., Marzoli, A., Bertrand, H., Chiaradia, M., Reisberg, L., Bellieni, G., Martins, L., Madeira, J., Mata, J., Youbi, N., De Min, A., Azevedo, M. R., & Bensalah, M. K. (2014). Enriched mantle source for the central Atlantic magmatic province: new supporting evidence from Southwestern Europe. *Lithos*, *188*, 15–32. https://doi.org/10.1016/j.lithos.2013.10.021

Casacão, J. (2015). *Tectono-Estratigrafia E Modelação De Sistemas Petrolíferos Da Bacia Do Porto*. Universidade de Lisboa.

Cebriá, J. M., López-Ruiz, J., Doblas, M., Martins, L. T., & Munhá, J. (2003). Geochemistry of the early jurassic messejana-plasencia dyke (Portugal-Spain); implications on the origin of the central Atlantic magmatic province. *Journal of Petrology*, *44*, 547–568. https://doi.org/10.1093/petrology/44.3.547

Cloetingh, S., Burov, E., Beekman, F., Andeweg, B., Andriessen, P. A. M., Garcia-Castellanos, D., de Vicente, G., & Vegas, R. (2002). Lithospheric folding in Iberia. *Tectonics*, *21*, 5-1–5-26. https://doi.org/10.1029/2001TC901031

Corti, G., Moratti, G., & Sani, F. (2005). Relations between surface faulting and granite intrusions in analogue models of strike-slip deformation. *Journal of Structural Geology*, *27*, 1547–1562. https://doi.org/10.1016/j.jsg.2005.05.011

Cunha, P. P. (2019). Cenozoic Basins of Western Iberia: Mondego, Lower Tejo and Alvalade Basins. In C. Quesada, & J. T. Oliveira (Eds.), *The Geology of Iberia: A Geodynamic Approach: Volume 4: Cenozoic Basins* (pp. 105–130). Springer International Publishing.

Cunha, T. A., Watts, A. B., Pinheiro, L. M., & Alves, T. M. (2009). *West Iberia margin subsidence-uplift history: constraints from seismic data and well and pseudo-well backstripping*. . 6 Simposio sobre el Margen Ibérico Atlántico

Dini, A., Westerman, D. S., Innocenti, F., & Rocchi, S. (2008). Magma emplacement in a transfer zone: the miocene mafic Orano dyke swarm of Elba Island, Tuscany, Italy. *Geological Society, London, Special Publications*, *302*, 131–148. https://doi.org/10.1144/SP302.10

Escada, C. (2019). *Post-Rift Magmatism on the Central West Iberian Margin (Estremadura Spur): New Evidences from Potential Field Data*. Universidade de Lisboa.

Escada, C., Santos, F., Represas, P., Pereira, R., Mata, J., Rosas, F., & Silva, B. (2019). Post-Rift Magmatism on the Central West Iberian Margin: New Evidence from Magnetic and Gravimetric Data Inversion in the Estremadura Spur. EGU General Assembly 2019, : Geophysical Research Abstracts.

Franke, D. (2013). Rifting, lithosphere breakup and volcanism: comparison of magma-poor and volcanic rifted margins. *Marine and Petroleum Geology*, *43*, 63–87. https://doi.org/10.1016/j.marpetgeo.2012.11.003

Geoffroy, L. (2005). Volcanic passive margins. *Comptes Rendus Geoscience*, *337*, 1395–1408. https://doi.org/10.1016/j.crte.2005.10.006

Gomes, A. S., Rosas, F. M., Duarte, J. C., Schellart, W. P., Almeida, J., Tomás, R., & Strak, V. (2019). Analogue modelling of brittle shear zone propagation across upper crustal morpho-rheological heterogeneities. *Journal of Structural Geology*, *126*, 175–197. https://doi.org/10.1016/j.jsg.2019.06.004

Gpep. (1986). *The Petroleum Potential of Portugal* (p. 62). Gabinete para a Pesquisa e Exploração de Petróleo.

Grange, M., Schärer, U., Cornen, G., & Girardeau, J. (2008). First alkaline magmatism during iberia-newfoundland rifting. *Terra Nova*, *20*, 494–503. https://doi.org/10.1111/j.1365-3121.2008.00847.x

Grange, M., Scharer, U., Merle, R., Girardeau, J., & Cornen, G. (2010). Plume-lithosphere interaction during migration of cretaceous alkaline magmatism in Sw Portugal: evidence from U-Pb Ages and Pb–Sr–Hf isotopes. *Journal of Petrology*, *51*, 1143–1170. https://doi.org/10.1093/petrology/egq018

Holford, S. P., Schofield, N., & Reynolds, P. (2017). Subsurface fluid flow focused by buried volcanoes in sedimentary basins: Evidence from 3D seismic data, bass basin, offshore Southeastern Australia. *Interpretation*, *5*, SK39–SK50. https://doi.org/10.1190/INT-2016-0205.1

Hubbard, R., Pape, J., & Roberts, D. E. (1985). Depositional Sequence Mapping as a Technique to Establish Tectonic and Stratigraphic Framework and Evaluate Hydrocarbon Potential on a Passive Continental Margin. In: O. R. Berg, & D. G. Woolverton (Ed.), *Seismic stratigraphy Ii: an integrated approach* (Vol. *39*, pp. 79-91). : American Association of Petroleum Geologists.

Inverno, C. M. C., Manupella, G., Zbyszewski, G., Pais, J., & Ribeiro, M. L. (1993) Notícia Explicativa Da Folha 42-C, Santiago Do Cacém, 1:50.000. Serviços geológicos de Portugal, Lisboa. 75.

Jackson, C.-A.-L., Schofield, N., & Golenkov, B. (2013). Geometry and controls on the development of igneous sill-related forced folds: a 2-D seismic reflection case study from offshore Southern Australia. *GSA Bulletin*, *125*, 1874–1890. https://doi.org/10.1130/B30833.1

Kullberg, J. C., Terrinha, P., Pais, J., Reis, R. P. D., & Legoinha, P. (2006). Arrábia E Sintra: Dois Exemplos De Tectónica Pós-Rifting Da Basia Lusitaniana. In: R. Dias, A. Araújo, P. Terrinha, & J. C. Kullberg (Ed.), *Geologia De Portugal No Contexto Da Ibéria* (pp. 369–395). Évora, Portugal: Universidade de Évora.

Kullberg, M. C., & Kullberg, J. C. (2000). Tectónica da região de sintra. *Memórias Geociências*, *2*, 1–34.

Llave, E., Hernández-Molina, F. J., García, M., Ercilla, G., Roque, C., Juan, C., Mena, A., Preu, B., Van Rooij, D., Rebesco, M., Brackenridge, R., Jané, G., Gómez-Ballesteros, M., & Stow, D. (2020). Contourites along the iberian continental margins: Conceptual and economic implications. *Geological Society, London, Special Publications*, *476*, 403.

Lneg-Lgm, (2010). Carta Geológica De Portugal. 1:000.000. LNEG-LGM.

Magee, C., Hunt-Stewart, E., & Jackson, C. A.- L. (2013). Volcano growth mechanisms and the role of sub-volcanic intrusions: Insights from 2d seismic reflection data. *Earth and Planetary Science Letters*, *373*, 41–53. https://doi.org/10.1016/j.epsl.2013.04.041

Magee, C., Jackson, C.-L., Hardman, J. P., & Reeve, M. T. (2017). Decoding sill emplacement and forced fold growth in the exmouth sub-basin, offshore northwest Australia: Implications for hydrocarbon exploration. *Interpretation*, *5*, SK11–SK22. https://doi.org/10.1190/INT-2016-0133.1

Manatschal, G., & Bernoulli, D. (1999). Architecture and evolution of nonvolcanic margins: present-day galicia and ancient adria. *Tectonics*, *18*, 1099–1119.

Martín-Chivelet, J., Floquet, M., García-Senz, J., Callapez, P. M., López-Mir, B., Muñoz, J. A., Barroso-Barcenilla, F., Segura, M., Soares, A. F., Dinis, P. M., Marques, J. F., & Arbués, P. (2019) Late cretaceous post-rift to convergence in Iberia. In: *The Geology of Iberia: A Geodynamic Approach* (Ed. by, Regional Geology Reviews, 3, 285–376. Springer.

Martins, L. T., Madeira, J., Youbi, N., Munhá, J., Mata, J., & Kerrich, R. (2008). Rift-related magmatism of the central Atlantic magmatic province in Algarve, Southern Portugal. *Lithos*, *101*, 102–124. https://doi.org/10.1016/j.lithos.2007.07.010

Mata, J., Alves, C. F., Martins, L., Miranda, R., Madeira, J., Pimentel, N., Martins, S., Azevedo, M. R., Youbi, N., De Min, A., Almeida, I. M., Bensalah, M. K., & Terrinha, P. (2015). $^{40}ar/^{39}ar$ ages and Petrogenesis of the west Iberian margin onshore magmatism at the Jurassic-cretaceous transition: geodynamic implications and assessment of open-system processes involving saline materials. *Lithos*, *236–237*, 156–172. https://doi.org/10.1016/j.lithos.2015.09.001

Mclean, C. E., Schofield, N., Brown, D. J., Jolley, D. W., & Reid, A. (2017). 3d seismic imaging of the shallow plumbing system beneath the ben nevis monogenetic volcanic field: Faroe-Shetland Basin. *Journal of the Geological Society*, *174*, 468. https://doi.org/10.1144/jgs2016-118

Merle, R. E., Jourdan, F., Chiaradia, M., Olierook, H. K. H., & Manatschal, G. (2019). Origin of widespread cretaceous alkaline magmatism in the Central Atlantic: a single melting anomaly? *Lithos*, *342–343*, 480–498. https://doi.org/10.1016/j.lithos.2019.06.002

Merle, R., Jourdan, F., Marzoli, A., Renne, P. R., Grange, M., & Girardeau, J. (2009). Evidence of multi-phase cretaceous to quaternary alkaline magmatism on tore-madeira rise and neighbouring seamounts from $^{40}ar/^{39}ar$ ages. *Journal of the Geological Society*, *166*, 879–894.

Miranda, R., Terrinha, P., Mata, J., Azevêdo, M. D. R., Chadwick, J., Lourenço, N., & Moreira, M. (2010). Caracterização Geoquímica Do Monte Submarino De Fontanelas, Margem Oeste Ibérica. X Congresso de geoquímica dos países de lingua oficial portuguesa, XVI Semana de geoquímica, Porto, Portugal, Universidade do Porto.

Miranda, R., Valadares, V., Terrinha, P., Mata, J., Azevedo, M. D. R., Gaspar, M., Kullberg, J. C., & Ribeiro, C. (2009). Age constrains on the late cretaceous alkaline magmatism on the west Iberian margin. *Cretaceous Research*, *30*, 575–586.

Montanari, D., Bonini, M., Corti, G., Agostini, A., & Del Ventisette, C. (2017). Forced folding above shallow magma intrusions: insights on supercritical fluid flow from analogue modelling. *Journal of Volcanology and Geothermal Research*, *345*, 67–80. https://doi.org/10.1016/j.jvolgeores.2017.07.022

Mougenot, D. (1980). Une Phase De Compression Au Crétacé Terminal À L'ouest Du Portugal: Quelques Arguments. Boletim da Sociedade Geológica de Portugal, XXII, 233-239.

Mougenot, D., Monteiro, J. H., Dupeuble, P. A., & Malod, J. A. (1979). La marge continentale sud-portugaise: évolution structurale et sédimentaire. *Ciências Da Terra*, *5*, 223–246.

Neres, M., Bouchez, J. L., Terrinha, P., Font, E., Moreira, M., Miranda, R., Launeau, P., & Carvallo, C. (2014). Magnetic fabric in a cretaceous sill (Foz Da Fonte, Portugal): Flow model and implications for regional magmatism. *Geophysical Journal International*, *199*, 78–101. https://doi.org/10.1093/gji/ggu250

Neres, M., Terrinha, P., Custódio, S., Silva, S. M., Luis, J., & Miranda, J. M. (2018). Geophysical evidence for a magmatic intrusion in the ocean-continent transition of the Sw Iberia margin. *Tectonophysics*, *744*, 118–133. https://doi.org/10.1016/j.tecto.2018.06.014

Peace, A. L., Welford, J. K., Ball, P. J., & Nirrengarten, M. (2019). Deformable plate tectonic models of the southern north Atlantic. *Journal of Geodynamics*, *128*, 11–37. https://doi.org/10.1016/j.jog.2019.05.005

Pereira, R., & Alves, T. M. (2011). Margin segmentation prior to continental break-up: a seismic-stratigraphic record of multiphased rifting in the North Atlantic. *Tectonophysics*, *505*, 17–34.

Pereira, R., & Alves, T. M. (2012). Tectono-Stratigraphic signature of multiphased rifting on divergent margins (Deep-Offshore Southwest Iberia, North Atlantic). *Tectonics*, *31*, TC4001. https://doi.org/10.1029/2011TC003001

Pereira, R., & Alves, T. M. (2013). Crustal deformation and submarine canyon incision in a meso-cenozoic first-order transfer zone (Sw Iberia, North Atlantic Ocean). *Tectonophysics*, *601*, 148–162. https://doi.org/10.1016/j.tecto.2013.05.007

Pereira, R., Alves, T. M., & Cartwright, J. (2011). Post-rift compression on the southwest iberian margin (Eastern North Atlantic): a case of prolonged inversion in the ocean-continent transition. *Journal of the Geological Society*, *168*, 1249–1263.

Pereira, R., Alves, T. M., & Mata, J. (2017). Alternating crustal architecture in West Iberia: A review of its significance in the context of ne Atlantic rifting. *Journal of the Geological Society*, *174*, 522–540. https://doi.org/10.1144/jgs2016-050

Pereira, R., & Barreto, P. (2018). Evidence and Significance of Buried Magmatic Features Offshore the West Iberian Margin. AAPG Europe Conference and Exhibition, Lisbon, Portugal.

Péron-Pinvidic, G., Manatschal, G., Masini, E., Sutra, E., Flament, J. M., Haupert, I., & Unternehr, P. (2015). Unravelling the along-strike variability of the Angola–Gabon rifted margin: A mapping approach. *Geological Society, London, Special Publications*, 438.

Péron-Pinvidic, G., Manatschal, G., & Osmundsen, P. T. (2013). Structural comparison of archetypal Atlantic rifted margins: A review of observations and concepts. *Marine and Petroleum Geology*, *43*, 21–47. https://doi.org/10.1016/j.marpetgeo.2013.02.002

Planke, S., Millett, J. M., Maharjan, D., Jerram, D. A., Abdelmalak, M. M., Groth, A., Hoffmann, J., Berndt, C., & Myklebust, R. (2017). Igneous seismic geomorphology of buried lava fields and coastal

escarpments on the vøring volcanic rifted margin. *Interpretation*, *5*, SK161–SK177. https://doi.org/10.1190/INT-2016-0164.1

Planke, S., Svensen, H., Myklebust, R., Bannister, S., Manton, B., & Lorenz, L. (2015) Geophysics and Remote Sensing. In: Physical Geology of Shallow Magmatic Systems (Ed. by, 131-146).

Ravnås, R., & Steel, R. J. (1998). Architecture of marine rift-basin successions. *AAPG Bulletin*, *82*, 110–146.

Rey, J., Dinis, J. L., Callapez, P., & Cunha, P. P. (2006). Da Rotura Continental À Margem Passiva: Composição E Evolução Do Cretácico De Portugal. INETI, Lisboa, Portugal. 75.

Ribeiro, A., Kullberg, M. C., Kullberg, J. C., Manuppella, G., & Phipps, S. (1990). A review of alpine tectonics in Portugal: Foreland detachment in basement and cover rocks. *Tectonophysics*, *184*, 357–366. https://doi.org/10.1016/0040-1951(90)90448-H

Ribeiro, P., Silva, P. F., Moita, P., Kratinová, Z., Marques, F. O., & Henry, B. (2013). Palaeomagnetism in the Sines Massif (Sw Iberia) revisited: Evidences for late cretaceous hydrothermal alteration and associated partial remagnetization. *Geophysical Journal International*, *195*, 176–191. https://doi.org/10.1093/gji/ggt261

Rock, N. M. S. (1982). The Late Cretaceous Alkaline Igneous Province in the Iberian Peninsula, and Its Tectonic Significance. *Lithos*, *15*, 111–131. https://doi.org/10.1016/0024-4937(82)90004-4

Roman-Berdiel, T., Gapais, D., & Brun, J. P. (1995). Analogue models of laccolith formation. *Journal of Structural Geology*, *17*, 1337–1346. https://doi.org/10.1016/0191-8141(95)00012-3

Schmiedel, T., Galland, O., & Breitkreuz, C. (2017). Dynamics of sill and laccolith emplacement in the brittle crust: role of host rock strength and deformation mode. *Journal of Geophysical Research: Solid Earth*, *122*, 8860–8871.

Sibuet, J.-C., Srivastava, S., & Manatschal, G. (2007). Exhumed mantle-forming transition crust in the newfoundland-iberia rift and associated magnetic anomalies. *Journal of Geophysical Research*, 112.

Silva, E. A., Miranda, J. M., Luis, J. F., & Galdeano, A. (2000). Correlation between the Palaeozoic Structures from West Iberian and Grand Banks Margins Using Inversion of Magnetic Anomalies. *Tectonophysics*, *321*, 57–71. https://doi.org/10.1016/S0040-1951(00)00080-9

Simões, P., Neres, M., & Terrinha, P. (2020). Joint Modeling of Seismic, Magnetic and Gravimetric Data Unravels the Extent of the Late Cretaceous Magmatic Province on the Estremadura Spur Offshore West Iberia. EGU General Assembly.

Soares, D. M., Alves, T. M., & Terrinha, P. (2012). The breakup sequence and associated lithospheric breakup surface: Their significance in the context of rifted continental margins (West Iberia and Newfoundland Margins, North Atlantic). *Earth and Planetary Science Letters*, *355–356*, 311–326. https://doi.org/10.1016/j.epsl.2012.08.036

Stapel, G., Cloetingh, S., & Pronk, B. (1996). Quantitative subsidence analysis of the Mesozoic evolution of the Lusitanian basin (Western Iberian Margin). *Tectonophysics*, *266*, 493–507. https://doi.org/10.1016/S0040-1951(96)00203-X

Sun, Q., Jackson, C.-L., Magee, C., Mitchell, S. J., & Xie, X. (2019). Extrusion dynamics of deepwater volcanoes revealed by 3-D seismic data. *Solid Earth*, *10*, 1269–1282. https://doi.org/10.5194/se-10-1269-2019

Sutra, E., Manatschal, G., Mohn, G., & Unternehr, P. (2013). Quantification and restoration of extensional deformation along the Western Iberia and Newfoundland Rifted Margins. *Geochemistry, Geophysics, Geosystems*, *14*, 2575–2597. https://doi.org/10.1002/ggge.20135

Teixeira, B. (2012) Modelação Da Subsidência, Evolução Térmica E Maturação De Intervalos Geradores Do Jurássico Na Bacia Lusitânica. : Universidade de Lisboa.

Terrinha, P., Pueyo, E. L., Aranguren, A., Kullberg, J. C., Kullberg, M. C., Casas-Sainz, A., & Azevedo, M. D. R. (2017). Gravimetric and magnetic fabric study of the sintra igneous complex: laccolith-plug emplacement in the western iberian passive margin. *International Journal of Earth Sciences*, *107*, 1807–1833. https://doi.org/10.1007/s00531-017-1573-7

Tucholke, B. E., Sawyer, D. S., & Sibuet, J. C. (2007). Breakup of the Newfoundland Iberia Rift. In: G. D. Karner, G. Manatschal, & L. M. Pinheiro (Eds.). *Imaging, Mapping and Modelling Continental Lithosphere Extension and Breakup*. *Geological Society, London*, *282*, 9–46.

Vanney, J. R., & Mougenot, D. (1990). Un Canyon Sous-Marin Du Type "Gouf': Le Canhão Da Nazare (Portugal). *Oceanologica Acta*, *13*, 1–14.

Vissers, R. L. M., & Meijer, P. T. (2012). Mesozoic rotation of Iberia: Subduction in the Pyrenees? *Earth-Science Reviews*, *110*, 93–110. https://doi.org/10.1016/j.earscirev.2011.11.001

Walker, F., Schofield, N., Millett, J., Jolley, D., Holford, S., Planke, S., Jerram, D. A., & Myklebust, R. (2020). Inside the Volcano: three-dimensional magmatic architecture of a buried shield volcano. *Geology*. https://doi.org/10.1130/g47941.1

Whitmarsh, R. B., Manatschal, G., & Minshull, T. A. (2001). Evolution of magma-poor continental margins from rifting to seafloor spreading. *Nature*, *413*, 150–154. https://doi.org/10.1038/35093085

Wilson, R. C. L. (1988). Mesozoic development of the Lusitanian Basin, Portugal. *Revista De La Sociedad Geologica De España*, *1*, 393–407.

Wilson, R. C. L., Manatschal, G., & Wise, S. (2001). Rifting Along Non-Volcanic Passive Margins: Stratigraphic and Seismic Evidence from the Mesozoic Successions of the Alps and Western Iberia. In R. C. L. Wilson, R. B. Whitmarsh, B. Taylor, & N. Froitzheim (Eds.), Non-volcanic rifting of the continental margins: a comparison of evidence from Land and Sea. *Geological Society, London*. *197*, 429-452.

Witt, W. G. (1977). Stratigraphy of the Lusitanian Basin, Shell Prospex Portuguesa, 61.

Zhao, F., Alves, T. M., Wu, S., Li, W., Huuse, M., Mi, L., Sun, Q., & Ma, B. (2016). Prolonged post-rift magmatism on highly extended crust of divergent continental margins (Baiyun Sag, South China Sea). *Earth and Planetary Science Letters*, *445*, 79–91. https://doi.org/10.1016/j.epsl.2016.04.001

SUPPORTING INFORMATION

Additional Supporting Information may be found online in the Supporting Information section.

How to cite this article: Pereira R, Rosas F, Mata J, Represas P, Escada C, Silva B. Interplay of tectonics and magmatism during post-rift inversion on the central West Iberian Margin (Estremadura Spur). *Basin Res*. 2021;33:1497–1519. https://doi.org/10.1111/bre.12524